REPORT 1338

NEAR NOISE FIELD OF A JET-ENGINE EXHAUST [1]

By Walton L. Howes, Edmund E. Callaghan, Willard D. Coles, and Harold R. Mull

SUMMARY

Aircraft structures located in the near noise field of a jet engine are subjected to extremely high fluctuating pressures that may cause structural fatigue. Studies of such structures have been limited by lack of knowledge of the loadings involved.

The acoustic near field produced by the exhaust of a stationary turbojet engine having a high pressure ratio was measured for a single operating condition without afterburning. The maximum over-all sound pressure without afterburning was found to be about 42 pounds per square foot along the jet boundary in the region immediately downstream of the jet-nozzle exit. With afterburning the maximum sound pressure was increased by 50 percent. The largest sound pressures without afterburning were obtained on a constant percentage band width basis in the frequency range from 350 to 700 cps.

Additional tests were made at a few points to find the effect of jet velocity on near-field sound pressures and to determine the difference in value between sound-pressure levels at rigid surfaces and corresponding free-field values. Near the jet nozzle, over-all sound pressures were found to vary as a low power (approx. unity) of the jet velocity. Over-all sound-pressure levels considerably greater than the corresponding free-field levels were recorded at the surface of a rigid plate placed along the jet boundary.

The downstream locations of the maximum sound pressure at any given frequency along the jet-engine-exhaust boundary and the longitudinal turbulent-velocity maximum of the same frequency along a small cold-air jet at 1 nozzle-exit radius from the jet axis were found to be nearly the same when compared on a dimensionless basis. Also, the Strouhal number of the corresponding spectra maximums was found to be nearly equal at similar distances downstream.

In addition to the magnitude and frequency distribution of the acoustic pressures, it is necessary to know the cross correlation of the pressure over the surface area. Cross-correlation measurements with microphones were made for a range of jet velocities at locations along the jet and at a distance from the jet. Free-field correlations of the over-all sound pressure and of the sound pressure in frequency bands from 100 to 1000 cps were obtained both longitudinally and laterally. In addition, correlations were obtained with microphones mounted at the surface of a rigid plate that was large compared with the distance over which a positive correlation existed.

The region of positive correlation was generally found to increase with distance downstream of the engine to 6.5 nozzle-exit diameters, but remained nearly constant thereafter. In general, little change in the correlation curves was found as a function of jet velocity or frequency-band width. The distance from unity correlation to the first zero correlation was greater for lateral than for longitudinal correlations for the same conditions and locations. The correlation curves obtained in free space and on the surface of the plate were generally similar.

The results are interpreted in terms of pressure loads on surfaces.

INTRODUCTION

The extremely intense acoustic radiation produced by a jet-engine exhaust has resulted in several serious problems. The far-field noise annoyance difficulties are well known (refs. 1 to 4). Another and perhaps more serious problem exists in the near noise field (refs. 5 and 6). Here, jet-induced acoustic pressure, particularly in the immediate vicinity of the exhaust, can be of sufficient magnitude to cause fatigue failure of adjacent surfaces. Moreover, these near-field sound pressures may produce harmful effects on ground and flight personnel if they are not shielded from the noise.

Because of the importance of these acoustic problems, the NACA Lewis laboratory has undertaken an experimental investigation of the character of the sound field near the exhaust of a full-scale engine.

The acoustic near field is a loosely defined region immediately surrounding any sound source or distribution of sources. Specifically, any point whose distance from an acoustic source is not large compared with the acoustic wavelength is said to be within the near field of the source. In the acoustic near field, sound pressures are not in phase with sound particle velocities.

Present knowledge of magnitudes and spectra of near-field jet noise from turbojet engines is quite limited. Data on the acoustic near field of air jets are reported in references 7 and 8. Noise surveys about jet engines are presented in references 9 and 10. The data on engine noise have been limited generally to distances greater than 10 feet from the jet-nozzle exit.

Jet-noise abatement at the source is the most desirable method for solving the structural and personnel problems. Knowledge of the space distribution of acoustic sources as to type, orientation, size, intensity, and frequency is important in connection with the noise-abatement problem Ultimately, a complete theory of jet noise is desired.

Any complete theoretical analysis of the jet as a noise source should be capable of predicting the sound pressures, spectra, and pressure correlations in space and time throughout the noise field. Lighthill has developed a basic theory of

[1] Supersedes NACA TN 3763, "Near Noise Field of a Jet-Engine Exhaust, I—Sound Pressures," by Walton L. Howes and Harold R. Mull, 1956, and NACA TN 3764, "Near Noise Field of a Jet-Engine Exhaust, II—Cross Correlation of Sound Pressures," by Edmund E. Callaghan, Walton L. Howes, and Willard D. Coles 1956.

aerodynamic noise (ref. 11) and, subsequently, has extended this theory (ref. 12) to explain the production of sound by jets for the subsonic regime. According to this theory, jet turbulence, particularly in regions of large mean shear (e. g., in the jet-mixing region), is a source of sound. In general, the jet can be subdivided into small volumes, which may be regarded as individual sources of sound. Each source is represented mathematically by an acoustic quadrupole, that is, a high-order source composed of four simple poles. Experimental measurements have borne out the more general predictions of Lighthill's theory. However, before any complete theory of jet noise can be confirmed, additional experimental data are required. Near-field jet noise represents one phase of the over-all problem that merits experimental investigation, not only to provide data for further theoretical development, but also to provide data relating to the structural problem.

This report contains results of a survey of near-field sound-pressure levels and spectra in the vicinity of the jet produced by a stationary axial-flow turbojet engine having a high pressure ratio across the jet nozzle. The data extend to within a few inches of the jet-nozzle exit and jet boundary. Except for ground reflection effects, the results are associated with free-field conditions. Some additional acoustic data obtained at the surface of a stiff plate and with afterburning are also included.

In order to calculate the stresses in a structure, it is necessary to know not only the acoustic pressures and spectra but also the space distribution of the pressures. In an essentially random acoustic field, such as that produced by a jet, the distribution of pressures over a surface is determined by correlation techniques. In this report, the application of correlation techniques to the determination of load distribution is discussed, and the results of correlation measurements in the near field are reported.

An electronic analog computer for determining correlation coefficients is described in appendix B by Channing C. Conger and Donald F. Berg.

Correlation measurements have been made both longitudinally and laterally with respect to the jet axis. The majority of the measurements were made with the microphones in free space. A single set of data is given with the microphones placed in a plate of fairly large dimensions.

SOUND PRESSURES

APPARATUS

The jet-noise measurements described in this report were obtained from the axial-flow turbojet engine shown in figure 1. This engine has a rated thrust of more than 10,000 pounds at sea-level static conditions and has a circular convergent nozzle. The engine was mounted in the thrust stand (shown in fig. 1) with its centerline 6 feet above ground level.

A 12-foot-high sound-absorbent wall composed of acoustic panels comprised the only large obstacle near the field of measurement. The wall was erected early in the program in order to reduce noise levels within the nearest buildings, which were about 1/10 mile forward of the engine. It was quite unlikely that the presence of the wall could affect noise levels in the field of measurement.

A block diagram of the sound analyzing equipment is shown in figure 2. The acoustic pickup consisted of a small condenser microphone and included preamplifier. The output from this unit is linear at all sound-pressure levels less than 180 decibels and is flat to within 1 decibel from 35 to 8000 cps. (Sound-pressure level in decibels in this report is based on a reference pressure of 2×10^{-4} dyne/cm^2.) Corrections for microphone response were applied to data for frequencies greater than 3000 cps. Power for the unit was obtained from a separate power supply. The power supply was kept in an acoustically treated box (fig. 3) in order to prevent its destruction by the intense noise. The output passed through a frequency-compensated cable to a ⅓-octave-band audiofrequency spectrometer and automatic recorder, which were located in a control room approximately 150 feet from the field of measurement. The recorder was of the quasi-peak-reading type. The useful frequency range of the entire unit was 35 to 15,000 cps. The entire system was calibrated to indicate the root-mean-square amplitude of a 400-cps sine wave signal supplied by a small calibrator loudspeaker driven by a transistor oscillator.

Sound-pressure levels were recorded in decibels. The recorded levels do not correspond to intensity levels because of the arbitrary phase relation between the sound-pressure and particle-velocity fluctuations in the acoustic near field.

The microphone unit was mounted on an extension arm from a remote-controlled motor-driven probe actuator. In addition, a second identical microphone was fixed at one end of the actuator support (fig. 3) for obtaining data at two points during short runs (e. g., during afterburning). The actuator allowed the microphone to be located at several points without stopping the engine. Successive positions of the microphone were remotely indicated within the control room. The actuator permitted a maximum linear traverse

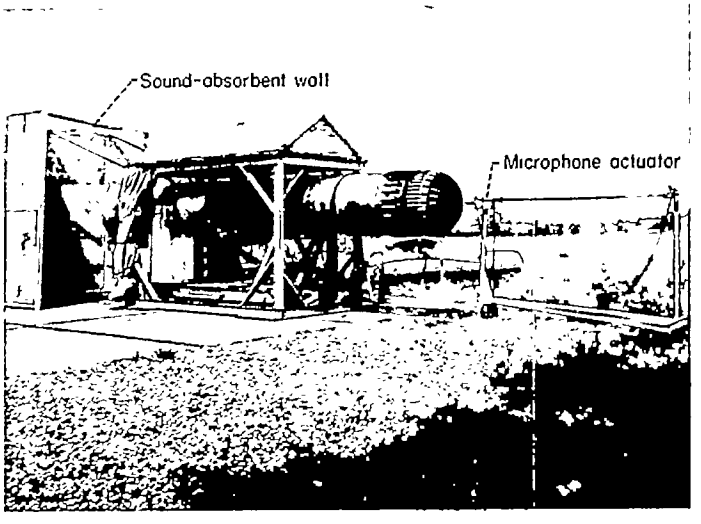

FIGURE 1.—Engine installation and microphone actuator.

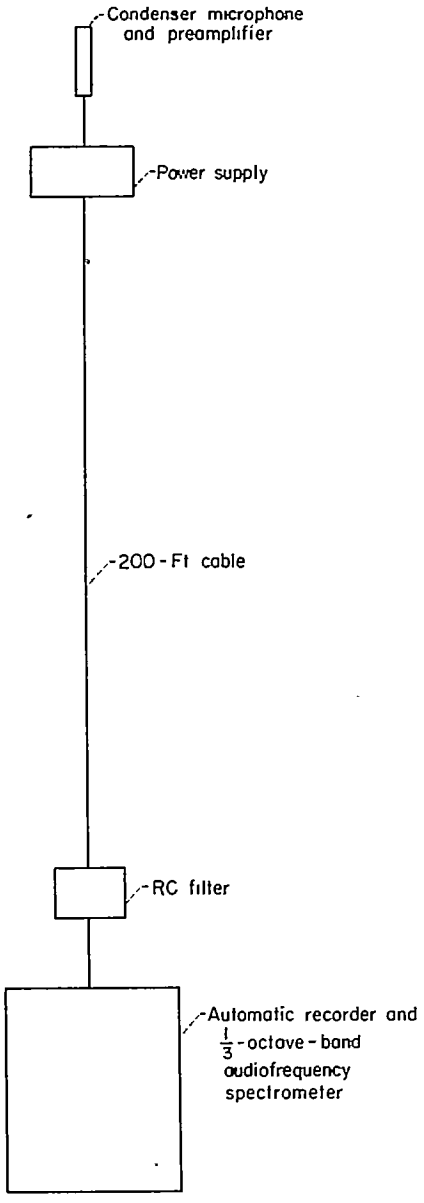

FIGURE 2.—Sound analyzing equipment.

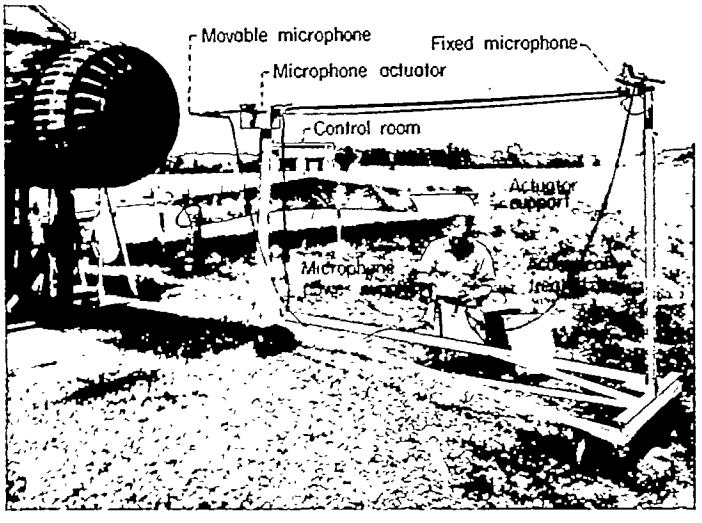

FIGURE 3.—Microphone actuator and support.

of the microphone of 8 feet without moving the actuator itself. The support was provided with various adjustments to permit the microphone to be kept in the horizontal plane containing the engine axis when the actuator was located over uneven ground.

PROCEDURE

The jet velocity and temperature profiles in the horizontal plane containing the engine axis were measured first in order to locate the jet boundary, that is, to determine how near the microphone could be brought to the jet without being affected by jet gusts or overheating. A string grid was laid out along the ground in order to locate points in the noise field.

Measured jet velocity and temperature boundaries for the fixed operating condition without afterburning are indicated in figure 4. In figure 4, abscissa values represent distances along the jet axis measured from the jet-nozzle exit. Ordinate values represent radial distances measured perpendicular to the jet axis and in the horizontal plane containing the jet axis. Indicated boundary values correspond to measurement stations at which average total pressures (velocity boundary) and average total temperatures were found to be within 0.05 inch of mercury and 5° F, respectively, of the ambient values. The solid line in figure 4 corresponds to the boundary of the noise measurements; that is, no noise measurements were made at stations corresponding to points below the solid line in figure 4. The boundary of the noise measurements was constructed at a slightly greater azimuth than those of the velocity and temperature boundaries in order to minimize the impingement of jet gusts upon the microphone in the presence of cross-winds. In particular, the boundary azimuth values measured with respect to the jet axis were as follows:

(1) Velocity boundary, ≈6.7°
(2) Temperature boundary, ≈9.4°
(3) Boundary of noise measurements, ≈9.8°

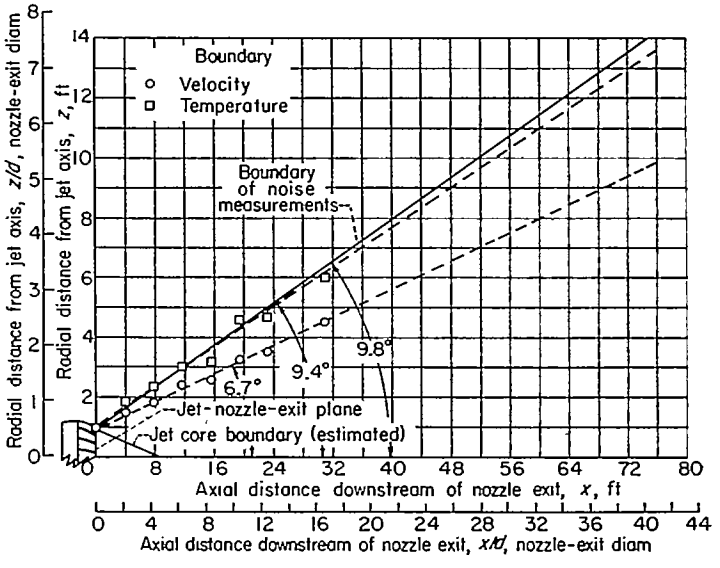

FIGURE 4.—Locus of jet velocity, temperature, and acoustic measurement boundaries.

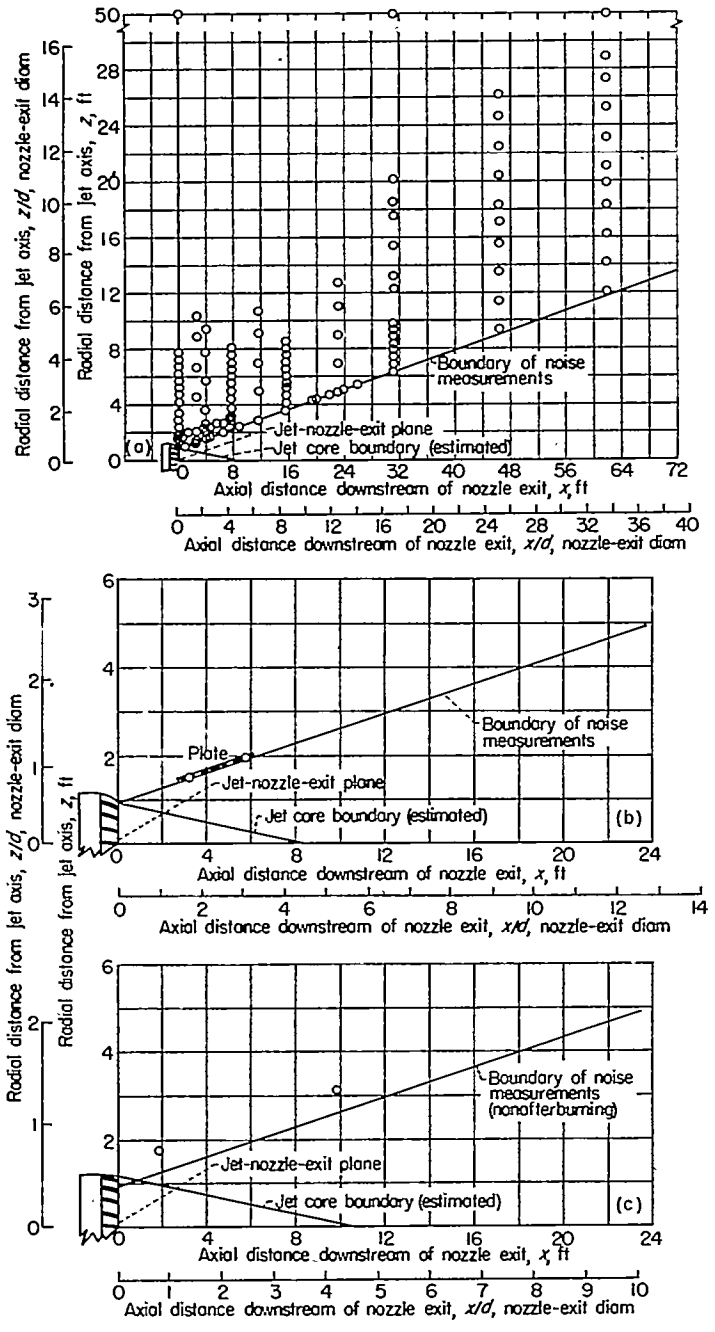

(a) Free field, fixed operating condition; nonafterburning.
(b) At plate surface; nonafterburning.
(c) Free field; afterburning.

FIGURE 5.—Locus of near-field-noise measurements.

Maps showing all points at which noise data were obtained comprise figure 5. The acoustic instrumentation was calibrated before each set of measurements.

The complete noise-field survey program extended over a period of several months. Engine operation was limited by poor weather conditions and the relative immobility of the microphone with respect to the size of the field to be surveyed. Therefore, repeatability of engine operating conditions was important for obtaining a complete field survey at a fixed operating condition.

Only one engine control variable is independent during static engine operation. Of the control variables, thrust, rotor speed, turbine-outlet temperature, and engine pressure ratio, measured engine thrust was selected as a convenient measure of repeatability. Engine thrust and the total acoustic power generated by turbulence (ref. 11) both depend to a different degree upon ambient temperature and pressure. Thus, constant engine thrust does not correspond to constant generated total acoustic power if ambient conditions change. Therefore, the effects of changes in ambient temperature and pressure on the measured sound field were necessarily regarded as uncorrectible errors.

The selected value of thrust and corresponding values of other significant parameters were as follows:

Thrust, lb	9600
Jet velocity, ft/sec	1850
Nozzle pressure ratio	2.2
Nozzle temperature ratio	2.8
Nozzle-exit diameter, ft	1.85

The jet velocity (a bulk velocity) was computed by dividing the measured value of thrust by the measured mass flow of gas through the engine. Good agreement between experimental data (ref. 13) and Lighthill's theoretical estimate (ref. 11) of the functional dependence of total acoustic power has been obtained by defining jet velocity in the preceding manner. The preceding values were repeatable for the entire range of ambient conditions encountered. The standard deviation of thrust and jet velocity resulting from all causes was about 1 percent and 20 feet per second, respectively.

In addition to the acoustic near-field survey at a fixed operating condition, measurements were made at a few points for various jet velocities without and with afterburning. Also, a few acoustic measurements were made at the surface of a stiff plate placed along the jet boundary in order to obtain an estimate of the increase of sound-pressure levels at rigid surfaces over the corresponding free-field values. The measurements at the plate surface were made for the same engine operating conditions listed previously. With afterburning, the values of the significant engine parameters were as follows:

Thrust, lb	14,750
Jet velocity, ft/sec	2,590
Nozzle-exit diameter, ft	2.33

Variations of experimental conditions resulted principally from wind, ambient temperature and pressure variations, and mislocation of the microphone. Tests were restricted to days on which wind velocities were less than 15 mph in order to minimize the influence of wind on the jet as a noise source. Accurate positioning of the microphone is particularly important in regions of large sound-pressure gradients. The microphone was located with respect to the nozzle exit to within 1 or 2 inches and was pointed directly at (normal to) the jet axis. The microphone height was set to within ¼ inch of the horizontal plane containing the engine axis.

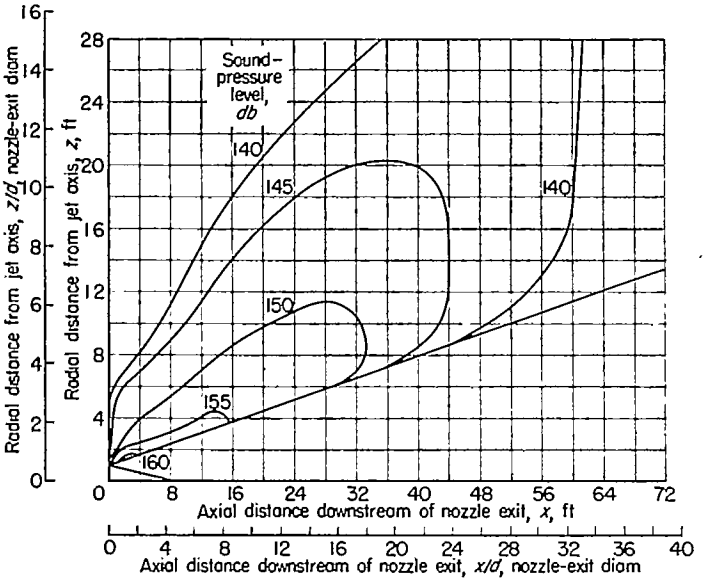

FIGURE 6.—Near-field contours of over-all sound-pressure level.

RESULTS

Contour maps showing lines of a constant sound-pressure level in the acoustic near field are presented in figures 6 and 7. The contour numbers denote (approx.) root-mean-square sound-pressure levels in decibels and are associated with an average engine thrust of 9600 pounds. The contours in figure 6 represent lines of constant over-all sound-pressure level that, for the tests described, included all frequencies between 35 and 15,000 cps. Corresponding maps for each ⅓-octave band in the frequency range from 35 to 11,200 cps are presented in figure 7. Figure 8 is provided as a convenience for comparing sound-pressure levels in decibels with sound pressures in pounds per square foot.

Free-field sound-pressure-level contours are shown in figures 6 and 7. Sound-pressure levels at surfaces may be considerably higher. For example, results presented in reference 8 and the additional tests performed using the engine described herein have revealed sound-pressure levels at the surface of a stiff plate considerably higher than the corresponding free-field values. As shown in figure 5 (b), the present plate tests were made at two stations along the jet boundary. At the upstream station, sound-pressure levels at the plate surface were found to be 2 or 3 decibels higher than the corresponding free-field values. However, at the downstream station, the increase was found to be as much as 16 decibels, probably resulting from impingement of the jet on the plate.

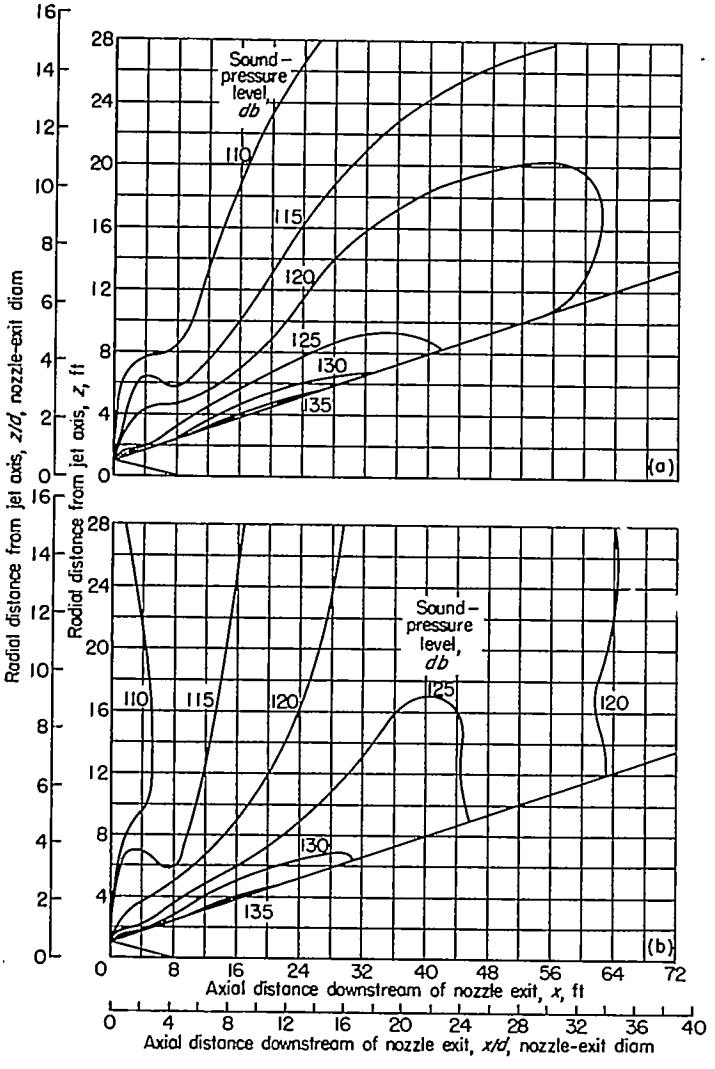

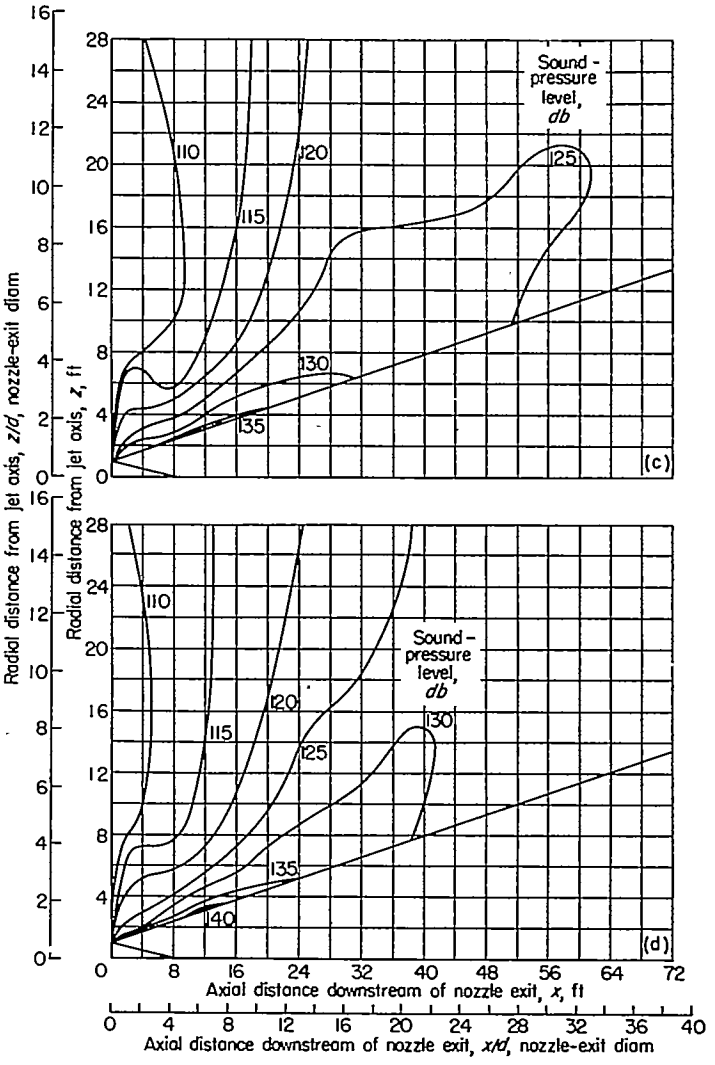

(a) Frequency band, 35 to 45 cps; Strouhal number, 0.035 to 0.045.
(b) Frequency band, 45 to 56 cps; Strouhal number, 0.045 to 0.056.
(c) Frequency band, 56 to 71 cps; Strouhal number, 0.056 to 0.071.
(d) Frequency band, 71 to 89 cps; Strouhal number, 0.071 to 0.089.

FIGURE 7—Near-field contours of 1/3-octave-band sound-pressure levels.

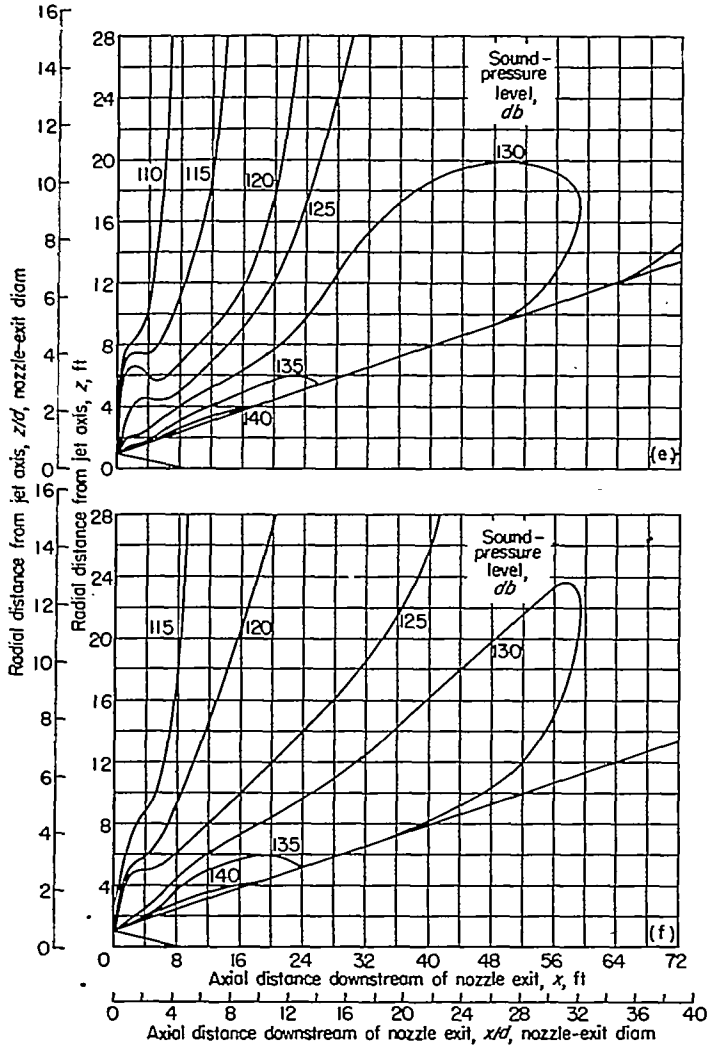

(e) Frequency band, 89 to 112 cps; Strouhal number, 0.089 to 0.112.
(f) Frequency band, 112 to 141 cps; Strouhal number, 0.112 to 0.141.

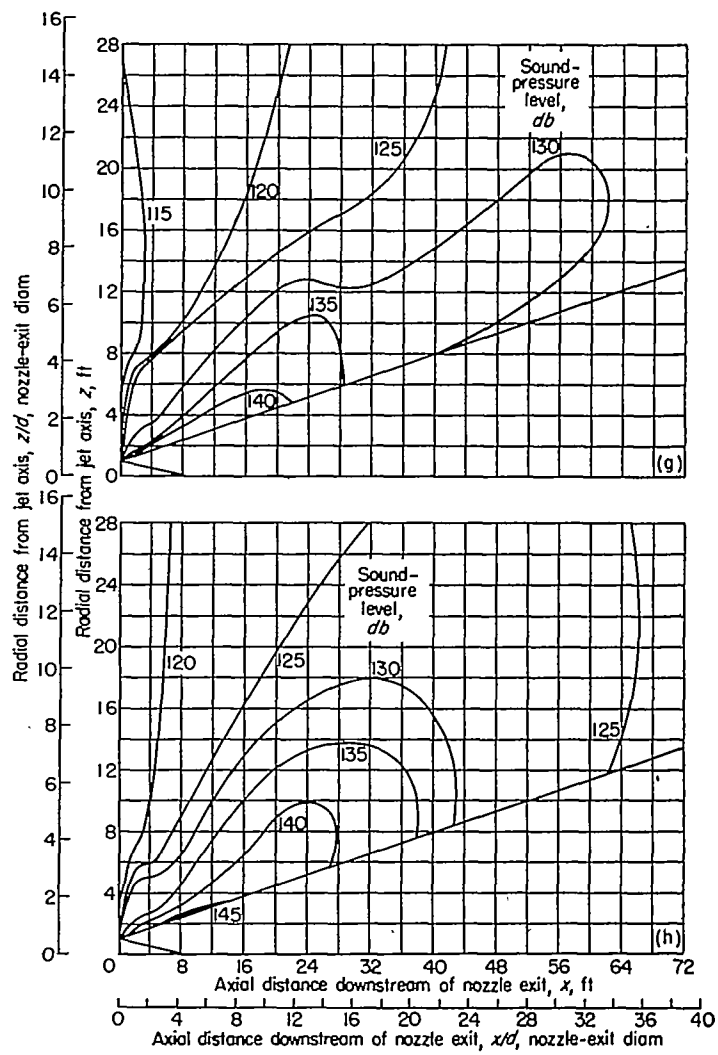

(g) Frequency band, 141 to 178 cps; Strouhal number, 0.141 to 0.178.
(h) Frequency band, 178 to 224 cps; Strouhal number, 0.178 to 0.224.

FIGURE 7.—Continued.

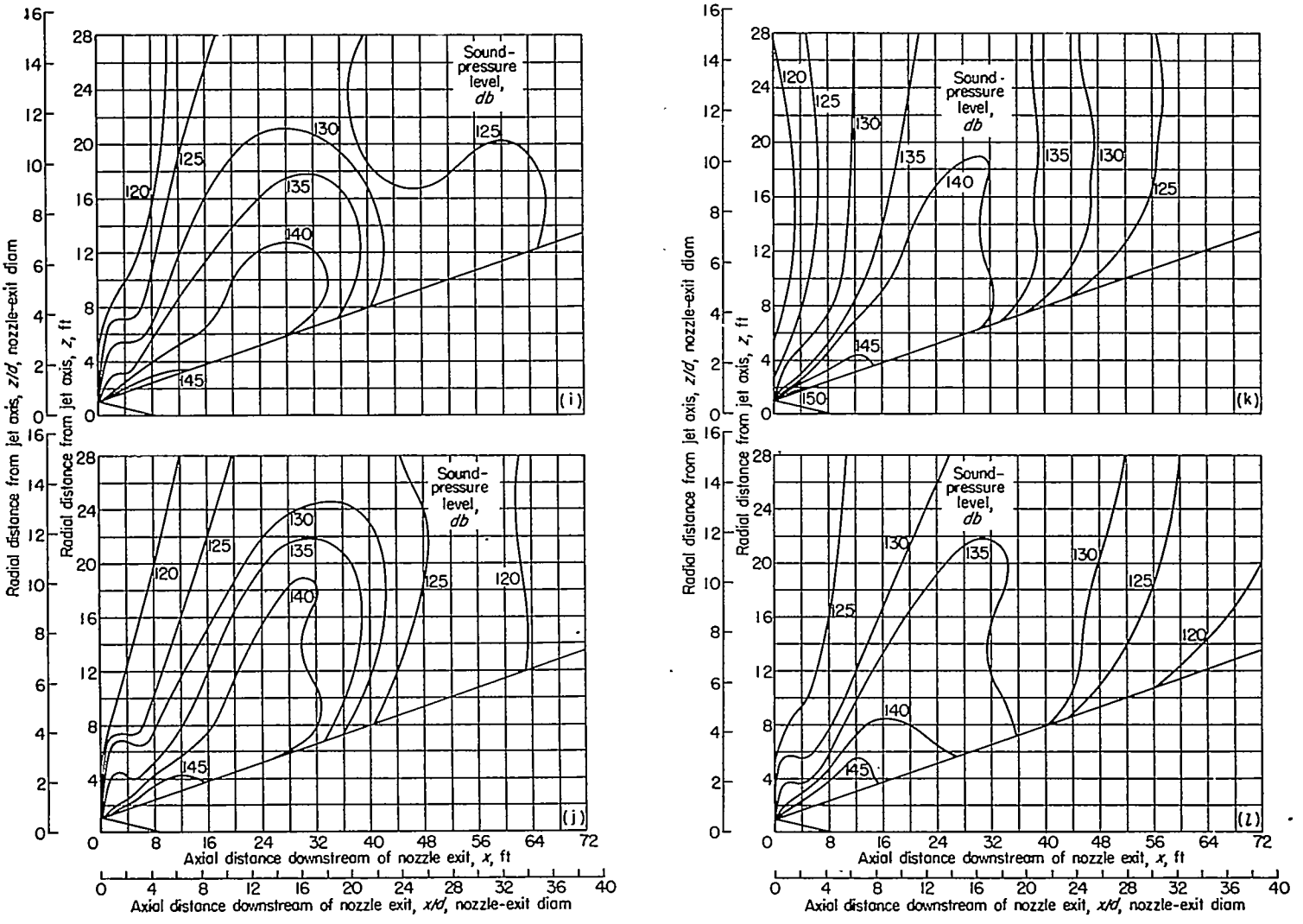

(i) Frequency band, 224 to 282 cps; Strouhal number, 0.224 to 0.282.

(j) Frequency band, 282 to 355 cps; Strouhal number, 0.282 to 0.355.

(k) Frequency band, 355 to 447 cps; Strouhal number, 0.355 to 0.447.

(l) Frequency band, 447 to 562 cps; Strouhal number, 0.447 to 0.562.

FIGURE 7.—Continued.

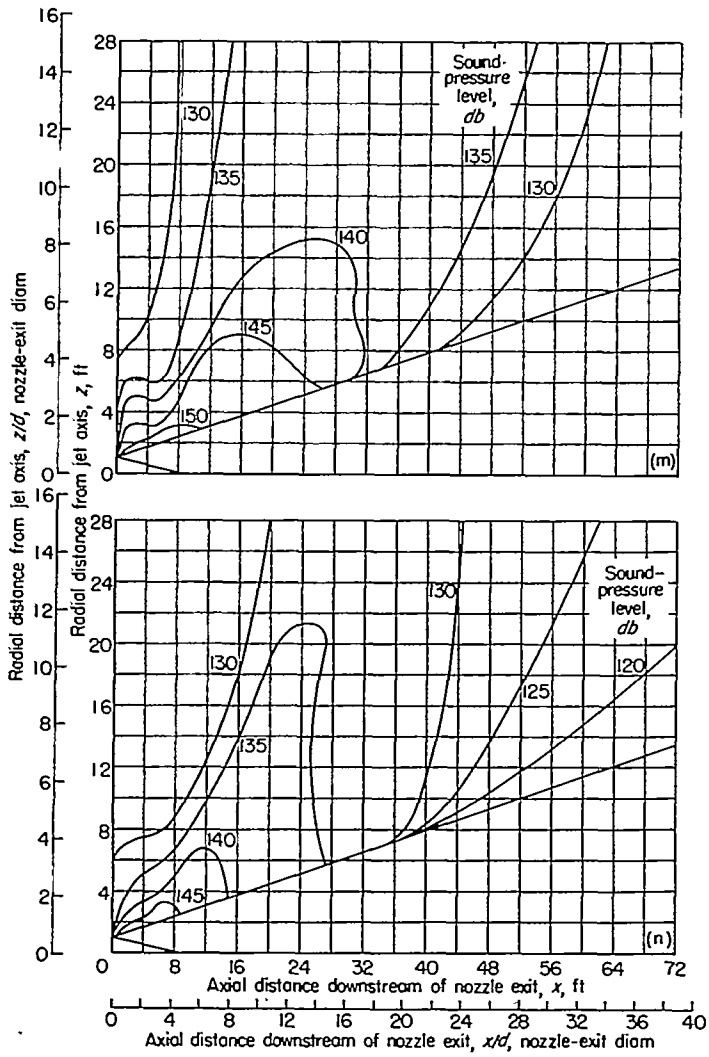

(m) Frequency band, 562 to 708 cps; Strouhal number, 0.562 to 0.708.

(n) Frequency band, 708 to 891 cps; Strouhal number, 0.708 to 0.891.

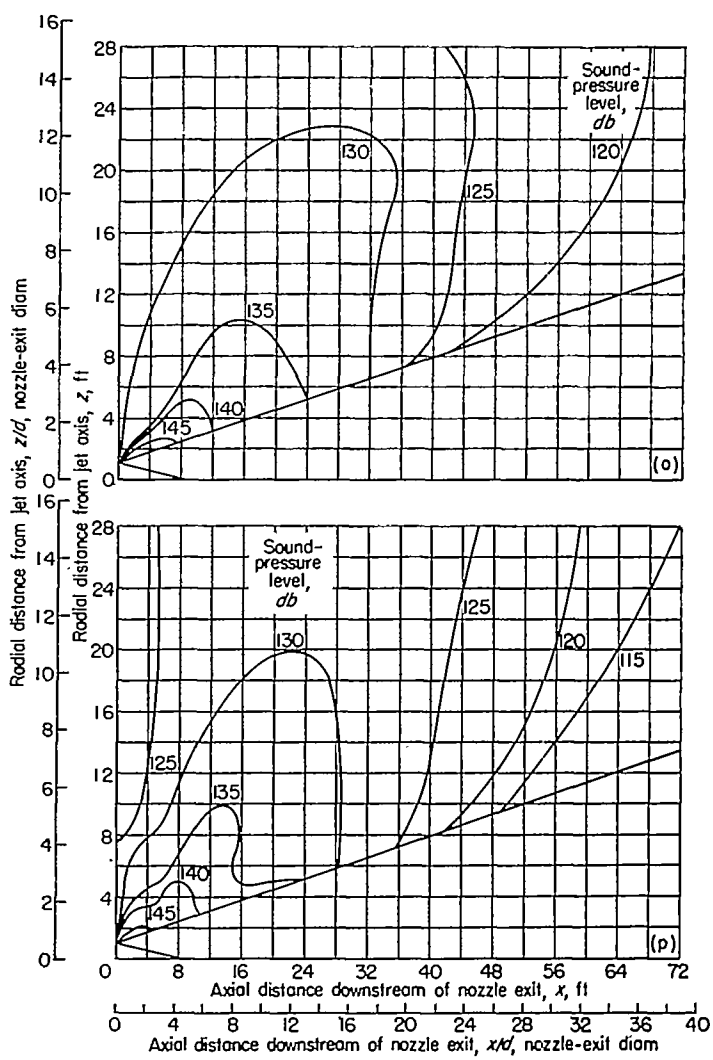

(o) Frequency band, 891 to 1120 cps; Strouhal number, 0.891 to 1.120.

(p) Frequency band, 1120 to 1410 cps; Strouhal number, 1.120 to 1.410.

FIGURE 7.—Continued.

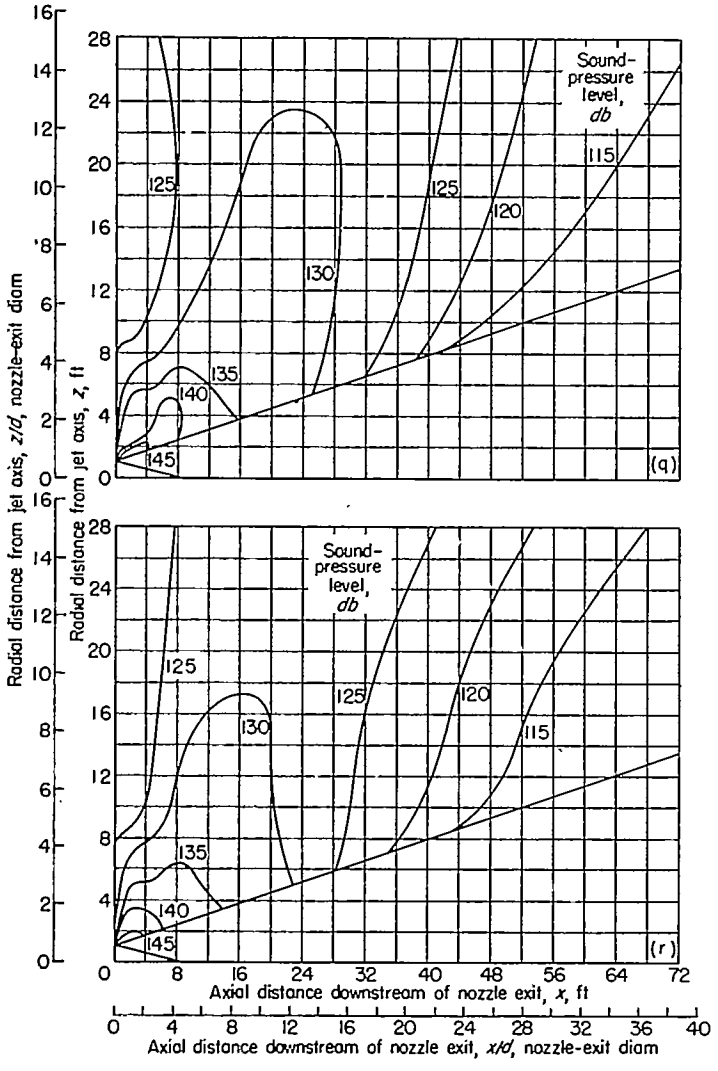

(q) Frequency band, 1410 to 1780 cps; Strouhal number, 1.410 to 1.780.

(r) Frequency band, 1780 to 2240 cps; Strouhal number, 1.780 to 2.240.

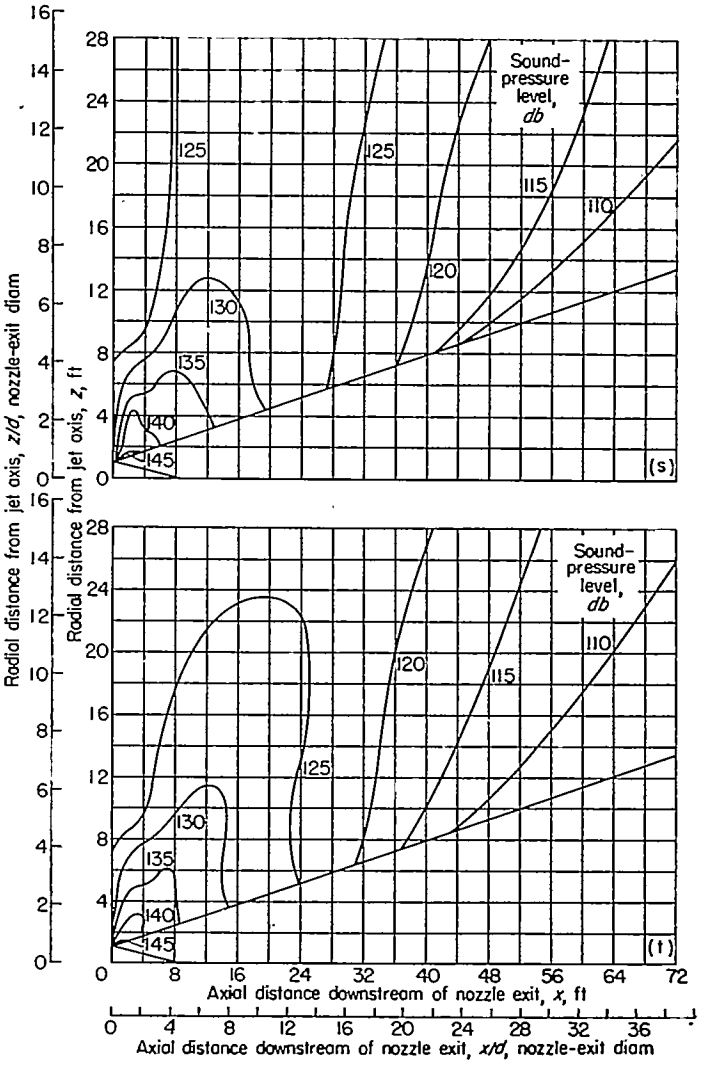

(s) Frequency band, 2240 to 2820 cps; Strouhal number, 2.240 to 2.820.

(t) Frequency band, 2820 to 3550 cps; Strouhal number, 2.820 to 3.550.

FIGURE 7.—Continued.

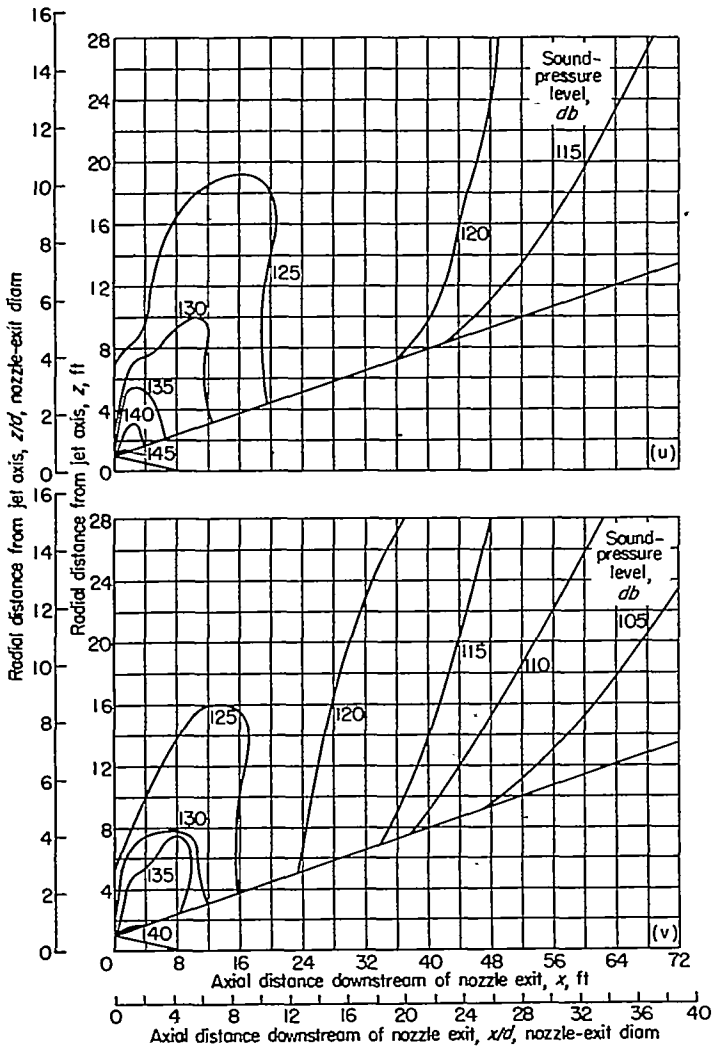

(u) Frequency band, 3550 to 4470 cps; Strouhal number, 3.550 to 4.470.

(v) Frequency band, 4470 to 5620 cps; Strouhal number, 4.470 to 5.620.

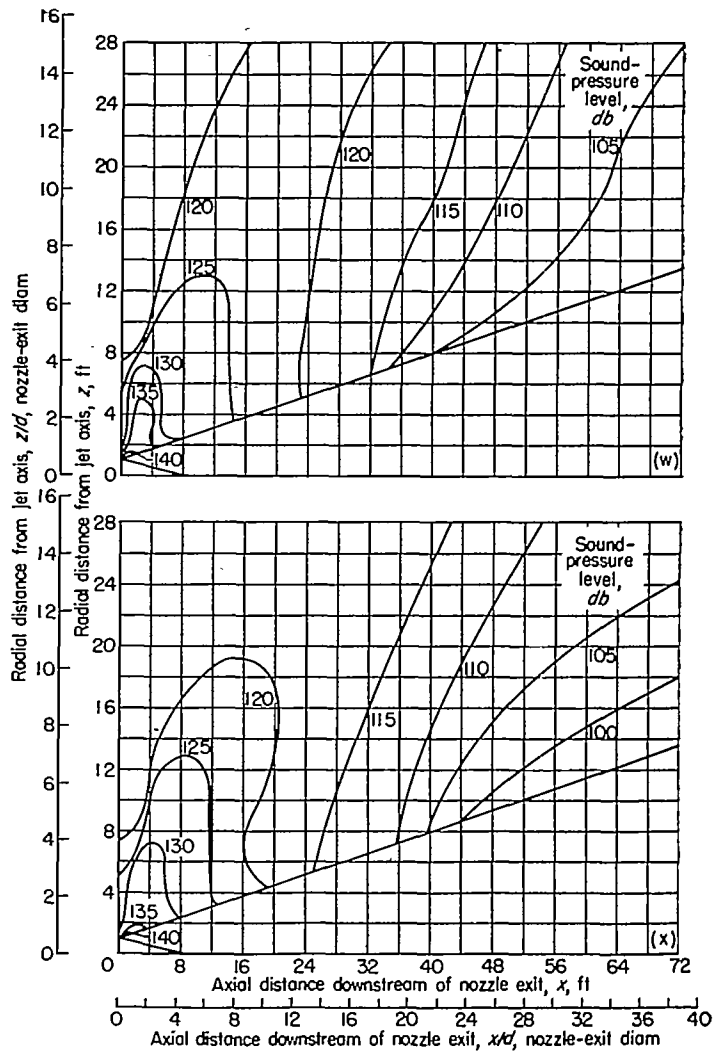

(w) Frequency band, 5620 to 7080 cps; Strouhal number, 5.620 to 7.080.

(x) Frequency band, 7080 to 8910 cps; Strouhal number, 7.080 to 8.910.

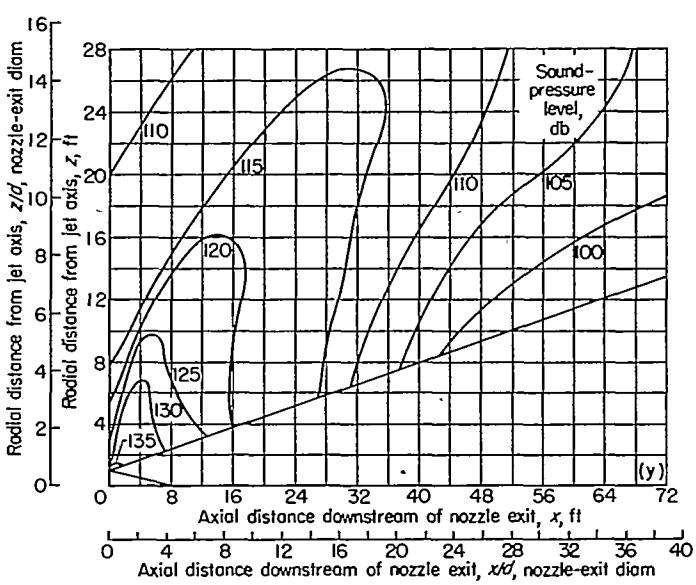

(y) Frequency band, 8910 to 11,200 cps; Strouhal number, 8.910 to 11.200.

FIGURE 7.—Concluded.

OVER-ALL SOUND PRESSURE

The measured maximum free-field over-all sound-pressure level without afterburning was approximately 160 decibels, which corresponds to a sound pressure of 42 pounds per square foot. This sound pressure was measured along the jet boundary from ½ to (at least) 2 nozzle-exit diameters from the nozzle exit (fig. 6). With afterburning the maximum sound-pressure level, determined from measurements at only two stations (fig. 5 (c)) along the jet boundary, was found to be 163.5 decibels at the upstream station. This level corresponds to a sound pressure of 63 pounds per square foot. At the downstream station the level was 160 decibels.

Considering only the free-field results without afterburning, the variation of over-all sound pressure along the jet boundary is shown in figure 9. The maximum sound pressure indicated in figure 9 is less than that indicated in figure 6 because of variations in experimental conditions, principally the ambient wind. Sound pressure, rather than sound-pressure level, was selected as the ordinate in figure 9 because sound pressure is probably more nearly proportional to acoustic-source strength within the jet.

According to figure 9, the over-all sound pressure along the boundary reached a maximum up to 4 diameters downstream of the nozzle exit, fell rapidly between 4 and 25 diameters downstream, and ceased to fall rapidly beyond 25 diameters downstream. Beyond this point, the sound-pressure level was at least 20 decibels below the maximum level.

The direction of maximum sound propagation was estimated from figure 6 to form an angle between 30° and 40° with respect to the jet axis. The point of maximum sound-pressure level, rather than the center of the nozzle exit, was used as the vertex in forming this angle. This result is in agreement with the results of far-field measurements (refs. 10 and 13).

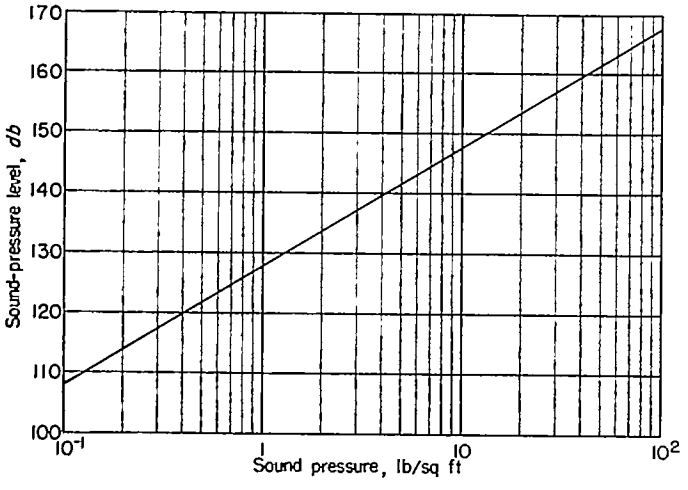

FIGURE 8.—Sound-pressure level as function of sound pressure.

Sound-pressure level (db) $= 20 \log \left(\frac{P}{P_o}\right)$. (Ref. pressure P_o, 2×10^{-4} dyne/cm².)

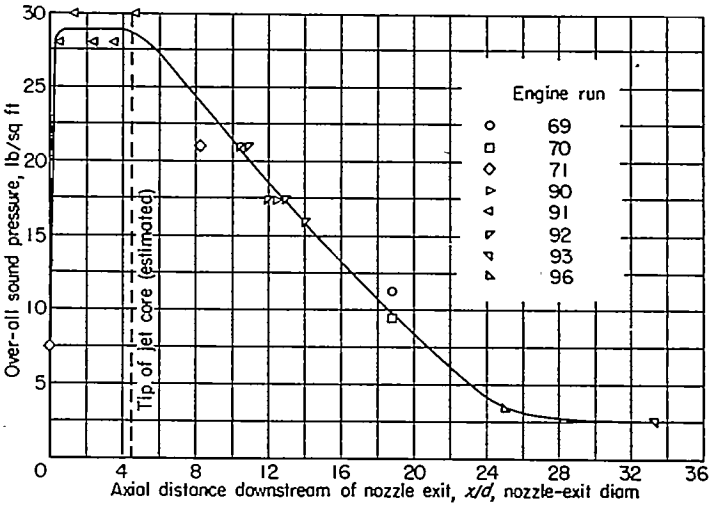

FIGURE 9.—Over-all sound pressure along jet boundary.

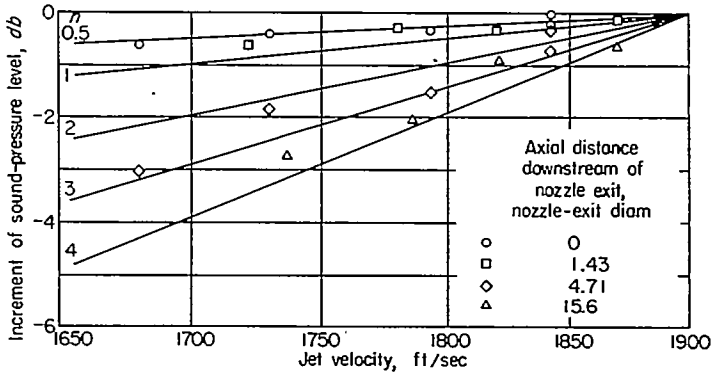

FIGURE 10.—Effect of jet velocity on over-all sound-pressure level along jet boundary.

The effect of jet velocity on over-all sound pressures at various points along the jet boundary is shown in figure 10. Lighthill's theory and experimental results (ref. 14) indicate that the relation between the averaged acoustic pressure P at a point and the jet velocity U is $P_2/P_1 = (U_2/U_1)^n$, where 1 and 2 are associated with different values of U. (All symbols are defined in appendix A.) Lines corresponding to various values of n are shown in figure 10. Near the nozzle $n < 1$, whereas beyond 15 diameters downstream $n \to 4$, which is approximately the value expected in the far field (refs. 11 and 12). Further experiments covering a wider range of velocities are required to establish accurately the variation of near-field sound pressures as a function of jet velocity.

SOUND-PRESSURE LEVEL IN FREQUENCY BANDS

The maximum sound-pressure level in any single ⅓-octave band was found to be about 150 decibels, which corresponds to a sound pressure of 13 pounds per square foot, in the three ⅓ octaves included in the interval from 350 to 700 cps. These levels were measured along the jet boundary from a point near the nozzle exit to 5.5 nozzle diameters downstream of the nozzle exit (figs. 7 (k), (l), and (m)).

The distribution along the jet boundary of the sound pressure in each frequency band was found to be useful for estimating the predominant location of acoustic sources of any given frequency. The apparent location of sources in

a selected frequency band was assumed to be at the same distance downstream as the maximum of the corresponding sound-pressure distribution curve. The frequency of acoustic sources as a function of distance downstream is denoted by the solid curve in figure 11. The dashed lines signify locations at which the sound-pressure level falls 6 decibels below the maximum level for the particular frequency. By replotting the data shown in figure 11 on a logarithmic scale, the relation between frequency of acoustic sources and distance downstream was found to be

$$\frac{fd}{U}=\left(1.25\frac{x}{d}\right)^{-1.22}.$$

The angle of maximum sound propagation was found from the acoustic maps in figure 7 to increase with increasing frequency from about 20° at 40 cps to 45° at 10,000 cps. The variation of angle of maximum propagation as a function of frequency is shown in figure 12.

SOUND-PRESSURE-LEVEL SPECTRA ALONG JET BOUNDARY

The sound field for particular frequency bands was considered in the preceding section. The same data are now reconsidered in terms of sound-pressure-level spectra at particular field points.

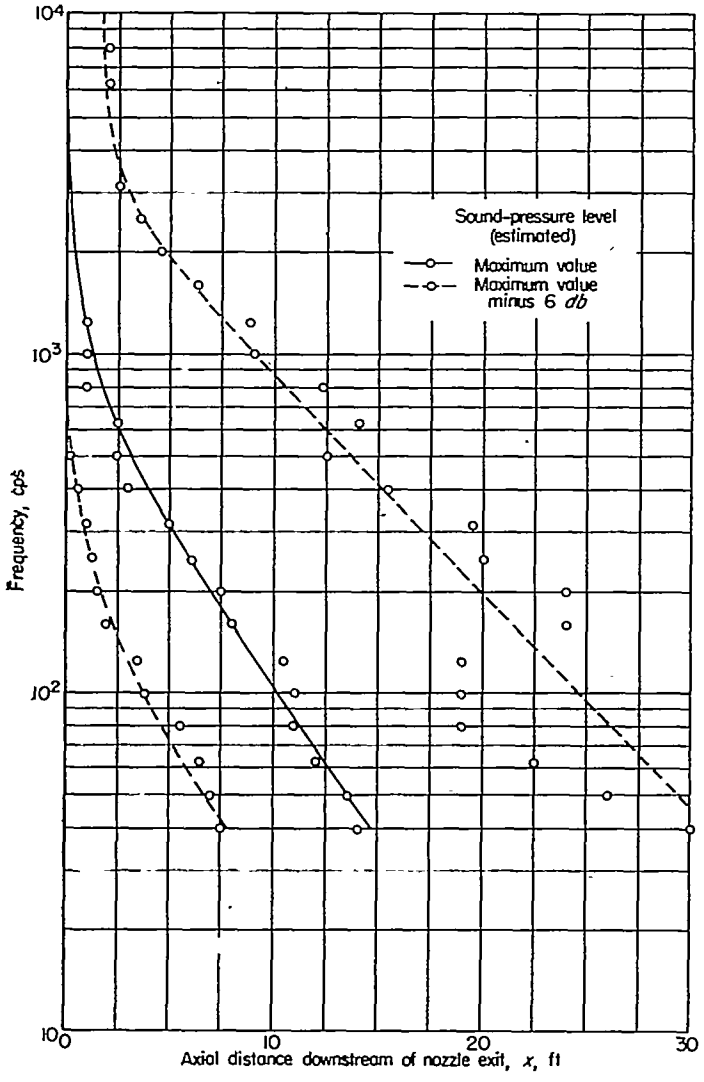

FIGURE 11.—Frequency of acoustic sources as function of distance downstream of jet-nozzle exit.

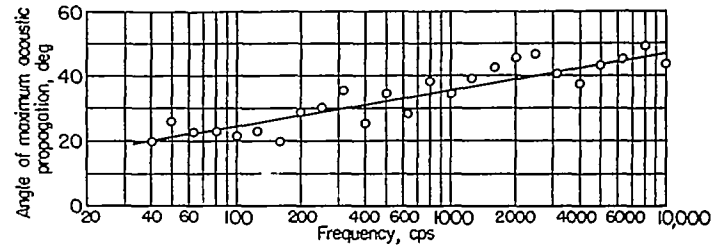

FIGURE 12.—Effect of frequency on angle of maximum acoustic propagation.

Spectra along the jet boundary from approximately ½ to 33 nozzle-exit diameters (0.83 to 61.8 ft) downstream of the nozzle exit are presented in figure 13. Each spectrum possesses a single peak in the audible frequency range. The variation of the frequency of peak sound-pressure level as a function of axial distance from the nozzle exit is shown in figure 14. The peak frequency was considered to correspond to the frequency at the intersection of the straight lines fitting the low- and high-frequency fall-off portions of the spectra in figure 13. Throughout the length of the mixing region, the relation between peak frequency and distance downstream of the nozzle exit is found from figure 14 to be $f=(5.6\times10^{-7}x)^{-0.48}$ where x is in feet and f is in cps. This result does not agree with the expression given in the preceding section for locating acoustic sources because the sound pressure is not uniformly distributed over all the frequency bands.

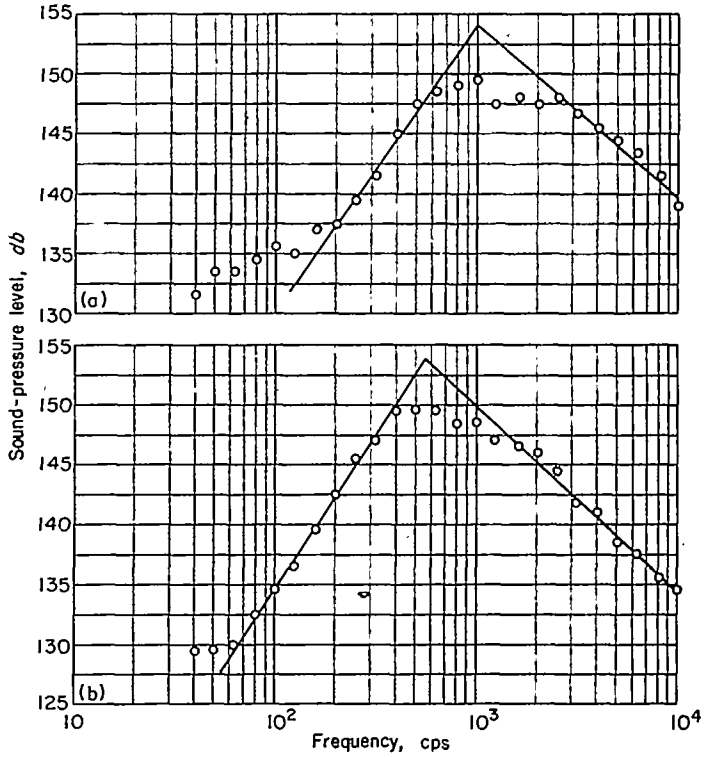

(a) Axial distance downstream of nozzle exit, 0.83 foot; over-all sound-pressure level, 156.5 decibels.
(b) Axial distance downstream of nozzle exit, 2.42 feet; over-all sound-pressure level, 157 decibels.

FIGURE 13.—Noise spectra along jet boundary.

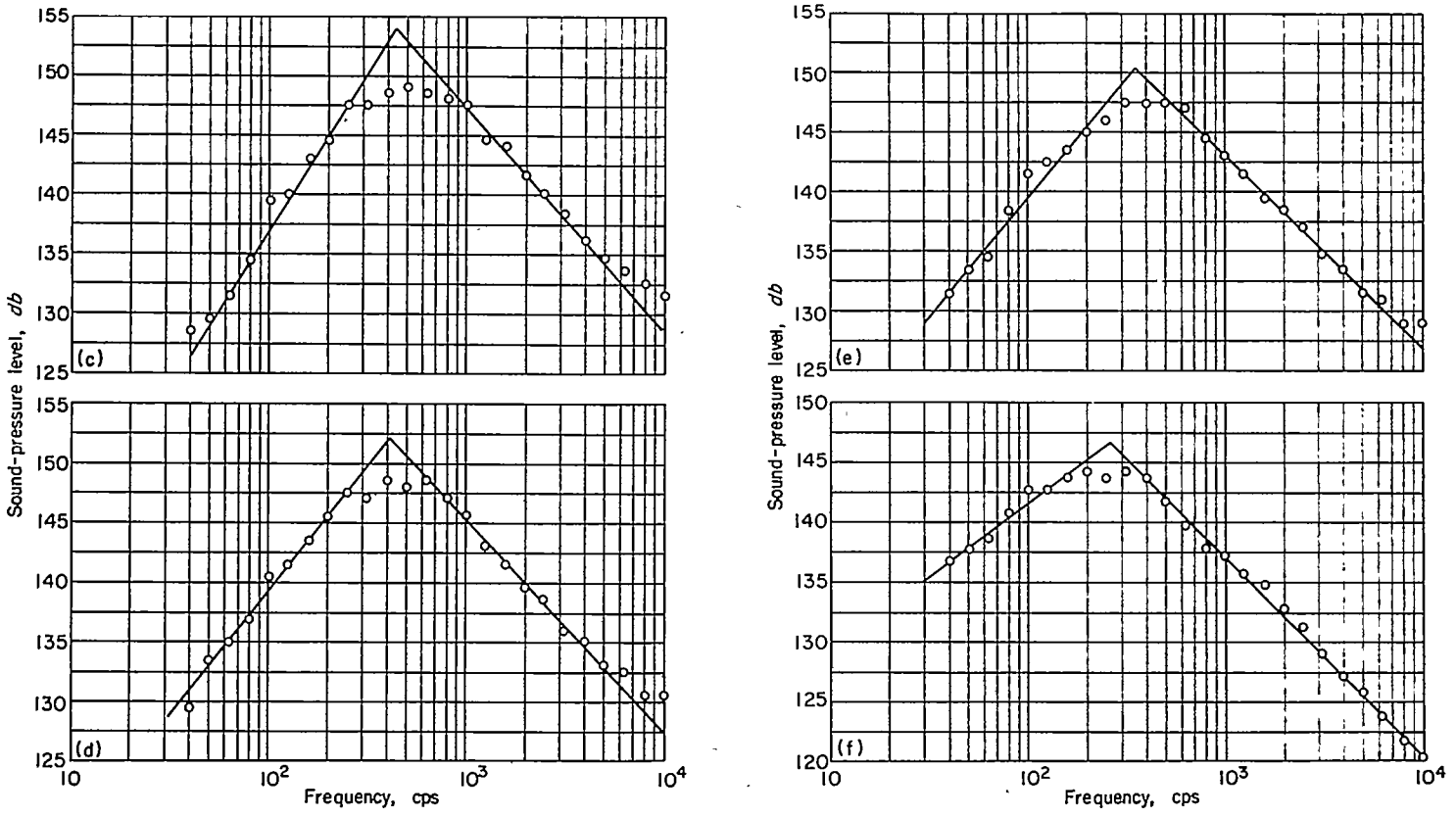

(c) Axial distance downstream of nozzle exit, 4.50 feet; over-all sound-pressure level, 156.5 decibels.

(d) Axial distance downstream of nozzle exit, 6.58 feet; over-all sound-pressure level, 156.5 decibels.

(e) Axial distance downstream of nozzle exit, 8.67 feet; over-all sound-pressure level, 157 decibels.

(f) Axial distance downstream of nozzle exit, 15.45 feet; over-all sound-pressure level, 154 decibles.

FIGURE 13.—Continued.

Up to about 3.5 nozzle-exit diameters downstream of the nozzle exit, the spectrum sound pressures fall off at the rate of 25 decibels per frequency decade on the low-frequency end and 15 decibels per decade on the high-frequency end (fig. 13). Beyond 5 diameters downstream of the nozzle exit, the low-frequency fall-off rate decreases to 15 or 20 decibels per decade, whereas the high-frequency fall-off rate remains unchanged.

SECOND-SOURCE NOISE

Profiles of sound-pressure levels along the jet boundary for each frequency band and the acoustic maps in figure 7 indicate the possible existence of a wide-frequency-band noise source in the vicinity of the jet-nozzle exit. Along the jet boundary this "second-source" noise is differentiable from the jet-induced noise only at frequencies less than 100 cps, as shown, for example, in figure 15. Moreover, the presence of secondary lobes in the acoustic maps (fig. 7) also indicates the existence of a second noise source. The second-source noise is probably shock-produced noise. The operational engine pressure ratio (2.2) is identical to that associated with the onset of shock-induced noise from small air jets (refs. 7 and 13). However, the maximum acoustic pressures in any frequency band which are attributable to the second source are appreciably less than those caused by the jet turbulence alone.

DISCUSSION

The results concerned with direction of maximum sound propagation, its variation with frequency, and the trend of the distribution according to frequency of acoustic sources along the jet are in general agreement with those presented in references 7 and 10. However, noise levels reported herein are considerably higher than the levels reported in reference 10, especially in regions nearest the jet nozzle. On the other hand, the present noise levels agree with the engine noise levels reported in reference 8.

Unfortunately, previously published data on the acoustic near field of jets are insufficient to permit comparison with the present results to more than a very limited extent. However, a considerable amount of jet-turbulence data for an unheated-air jet issuing from a circular convergent nozzle is given in reference 15. Comparing the air-jet turbulence data in reference 15 with the jet-engine acoustic data is of interest in attempting to relate jet-engine sound fields to those of air jets and in relating turbulence to sound. Two comparisons were made:

(1) Comparison of the distance downstream of sound-pressure and longitudinal turbulent-velocity maximums for each ⅓-octave band

(2) Comparison of the frequencies of the sound-pressure-spectrum and longitudinal turbulent-velocity-spectrum maximums as a function of distance downstream

The values of the significant parameters associated with the air-jet turbulence data in reference 15 are

Jet velocity, ft/sec	342
Nozzle pressure ratio	1.06
Nozzle temperature ratio	1.01
Nozzle-exit diameter, in	3.5

Because these values differed greatly from those associated with the engine acoustic data, the preceding comparisons were made, as suggested by the work of Lighthill and Greatrex, on the basis of Strouhal number (based on jet bulk velocity and nozzle-exit diam.) rather than frequency, and distances downstream were expressed in jet-nozzle-exit diameters. The comparisons were made between noise measured along the jet boundary and turbulence measured along the jet length at a distance of 1 nozzle-exit radius from the jet axis. At distances less than 20 nozzle-exit diameters downstream of the nozzle exit, the over-all longitudinal turbulent-velocity fluctuations are a maximum at about 1 nozzle-exit radius from the jet axis (ref. 15).

The results of the comparisons are presented in figures 16 and 17. In figure 16, the Strouhal numbers of the sound-pressure and longitudinal turbulent-velocity maximums are plotted as a function of distance downstream of the nozzle exit in nozzle-exit diameters. A similar plot which locates the frequencies of the corresponding spectra maximums is shown in figure 17. The acoustic and turbulence spectra (in terms of Strouhal number, rather than frequency) at corresponding dimensionless distances downstream are compared in figure 18.

The good agreement between the curves for sound and turbulence in figure 16 is appreciably better than that which resulted when frequency, rather than Strouhal number, was adopted as the ordinate. The present result indicates that frequencies of turbulent-velocity fluctuations are associated with noise of the same frequency. (The same conclusion is reached in ref. 16 from theoretical considerations.) Moreover, the distribution according to frequency of acoustic sources in the air jet was similar to that in the jet-engine exhaust. The distribution was relatively independent of

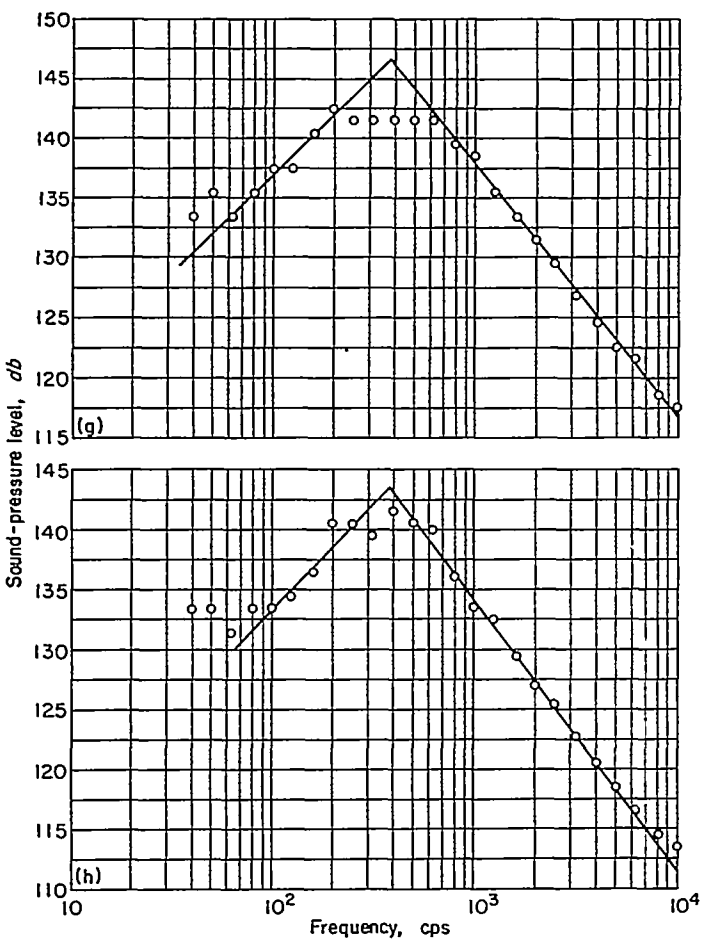

(g) Axial distance downstream of nozzle exit, 20 feet; over-all sound-pressure level, 154 decibels.

(h) Axial distance downstream of nozzle exit, 26 feet; over-all sound-pressure level, 151.5 decibels.

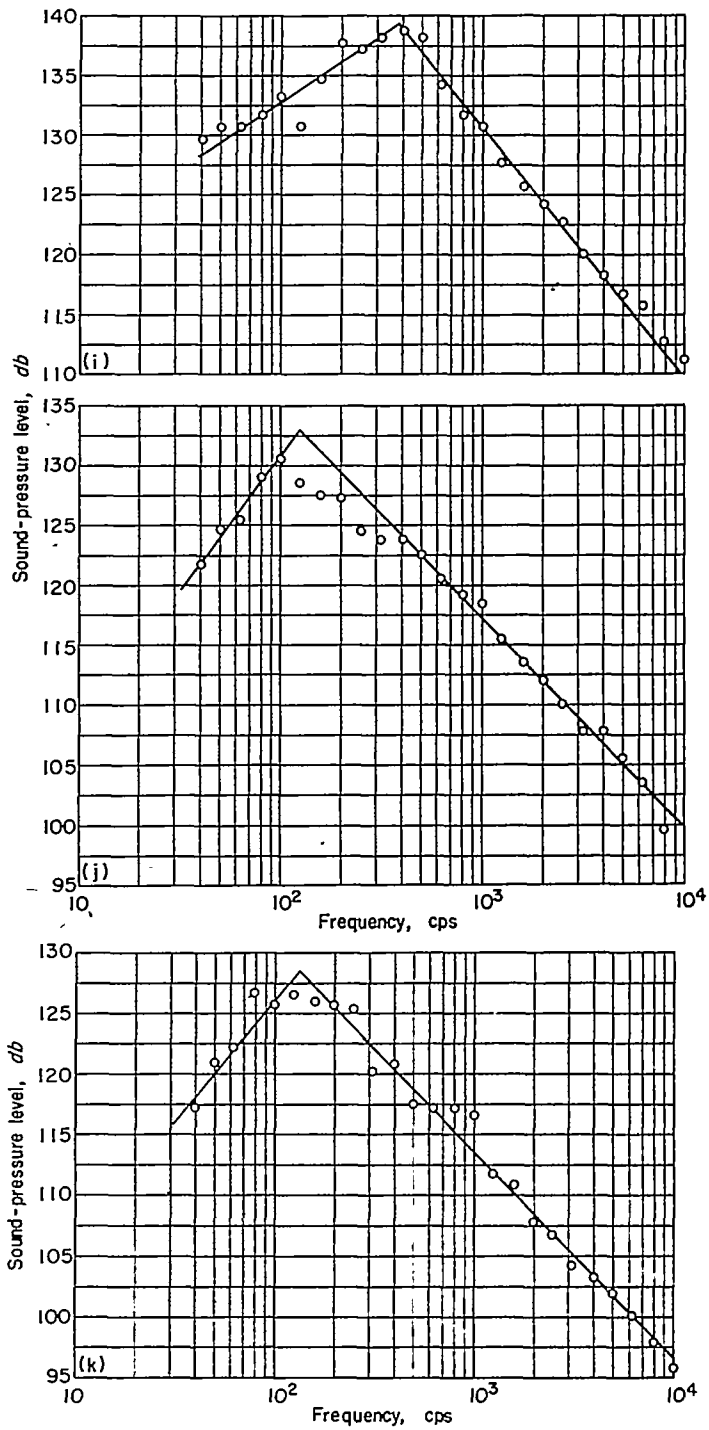

(i) Axial distance downstream of nozzle exit, 30.9 feet; over-all sound-pressure level, 148.5 decibels.

(j) Axial distance downstream of nozzle exit, 46.35 feet; over-all sound-pressure level, 138.5 decibels.

(k) Axial distance downstream of nozzle exit, 61.8 feet; over-all sound-pressure level, 135.5 decibels.

FIGURE 13.—Concluded.

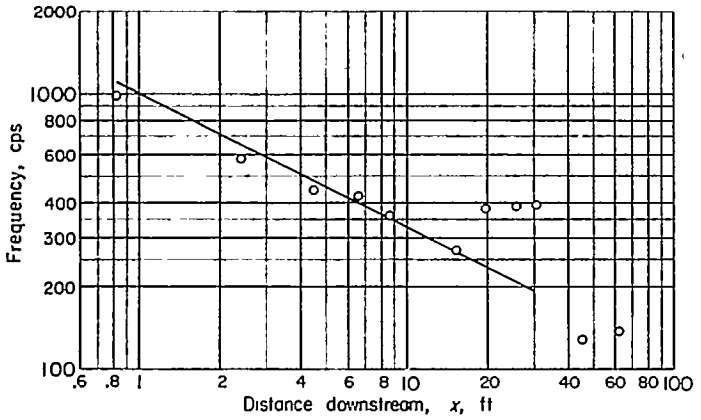

FIGURE 14.—Frequency of acoustic spectrum maximum as function of distance downstream of jet-nozzle exit.

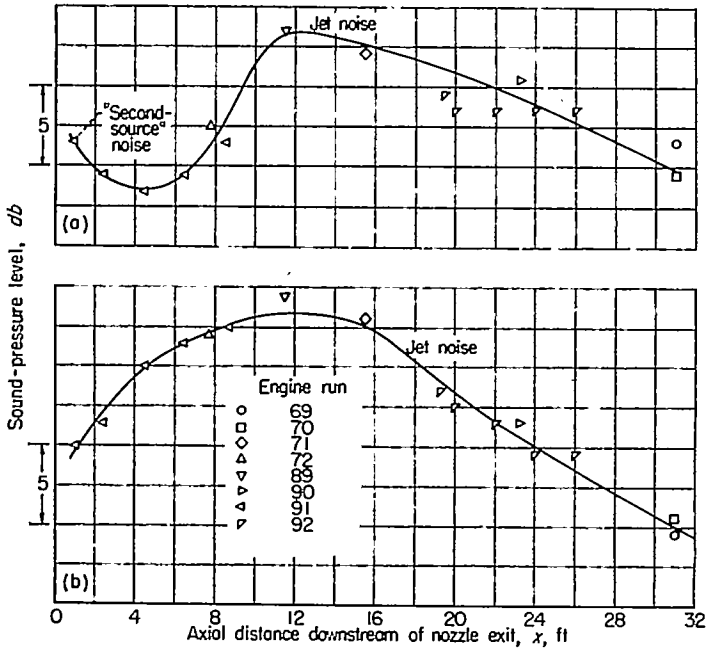

(a) Frequency band, 35 to 45 cps.
(b) Frequency band, 112 to 141 cps.

FIGURE 15.—Sound-pressure level along jet boundary.

jet temperature. Peak noise and turbulence at frequencies corresponding to values of Strouhal number larger than 0.15 occurred upstream of the tip of the jet core ($x/d<4.5$), that is, in the jet-mixing region.

A comparison of the acoustic and turbulence spectra of figure 18 shows that, in general, the acoustic spectra are more peaked. The differences in slope are rather small near the jet exit (small values of x/d), but become larger downstream. This is the effect which occurs with a quadrupole source of sound. Very near the source, the sound pressures vary as the square of the velocity fluctuations, whereas far from the source, the sound pressures vary as the fourth power of the jet velocity fluctuations. For positions near the jet exit the microphone is located very close to the position of maximum turbulent intensity. Downstream the microphone is located at a distance from the position of maximum intensity. The increase in distance between the source, or the maximum intensity of turbulence in the jet, and the microphone position probably causes the

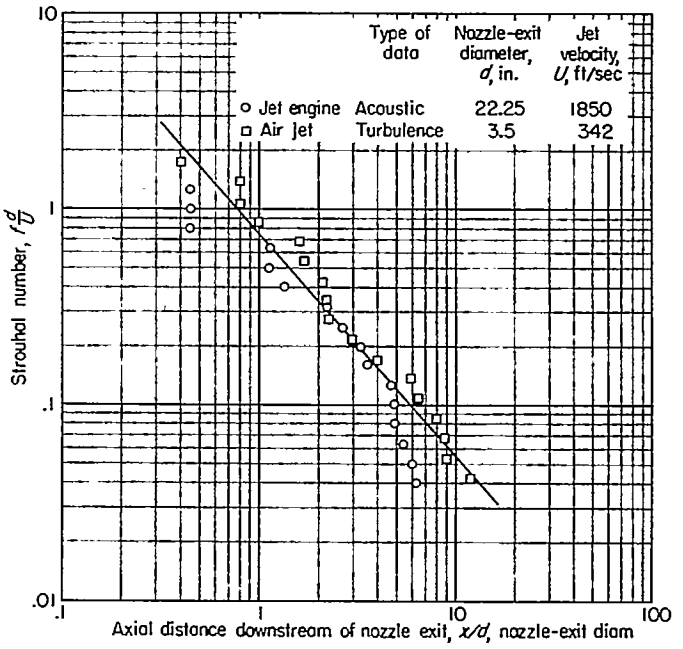

FIGURE 16.—Downstream location of maximum acoustic pressure and longitudinal-turbulence intensity for given frequencies. Comparison of jet-engine and air-jet data.

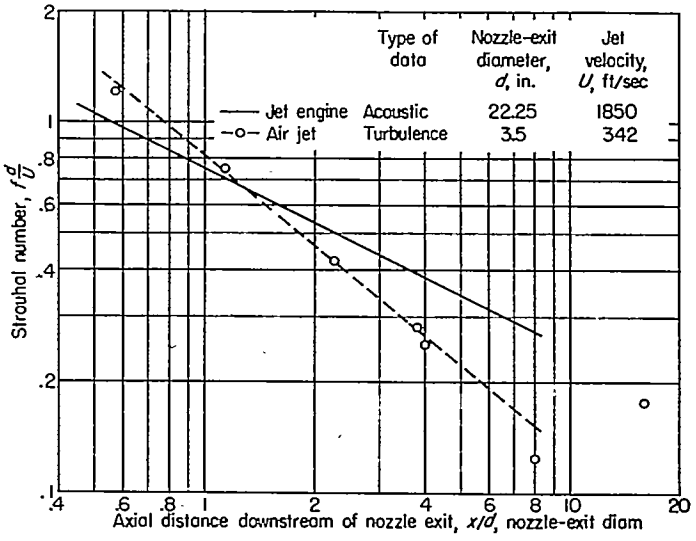

FIGURE 17.—Comparison of Strouhal numbers of acoustic and turbulence spectra maximums as function of dimensionless distance downstream of jet-nozzle exit.

increased peaking of the acoustic spectra with downstream position.

As shown in figure 17, the maximum of the acoustic spectra varies less as a function of distance downstream than does the corresponding maximum of the turbulent-velocity spectra. The effect amounts to stretching, in the flow direction, the jet-flow field of the engine with respect to that of the air jet. The effect is not one of temperature because the velocity field of a jet becomes compressed longitudinally as the jet temperature is increased (see figs. 7 and 10 of ref. 17). Rather, choking of the jet, which commences at a nozzle pressure ratio of 1.89, appears to explain the stretching of the engine flow field. In the presence of choking, the rate of expansion of the mixing region is less than for unchoked conditions (ref. 18).

Comparing the downstream distance of the acoustic and turbulence maximums for a given frequency is not the same as comparing the frequency of the corresponding spectra maximums at the same distance downstream of the nozzle exit, because the maximum level and spectrum maximum for a given frequency may not occur at the same distance downstream. Comparisons of the frequencies of spectra maximums at the same distance downstream are made in references 15 and 19. However, comparing the locations of the maximum levels associated with a given frequency (fig. 16) is more directly related to locating acoustic sources according to frequency.

Although the maximum over-all turbulence occurs at about 1 nozzle-exit radius from the jet axis, the maximum turbulence at a specified frequency may not occur at 1 nozzle-exit radius. Therefore, the entire field of turbulence should be taken into account in determining the location of the turbulence maximum for a given frequency. In comparing this location with the acoustic results, the distance of the turbulence maximum from the jet boundary should also be considered. In the present comparisons, the two preceding effects were disregarded.

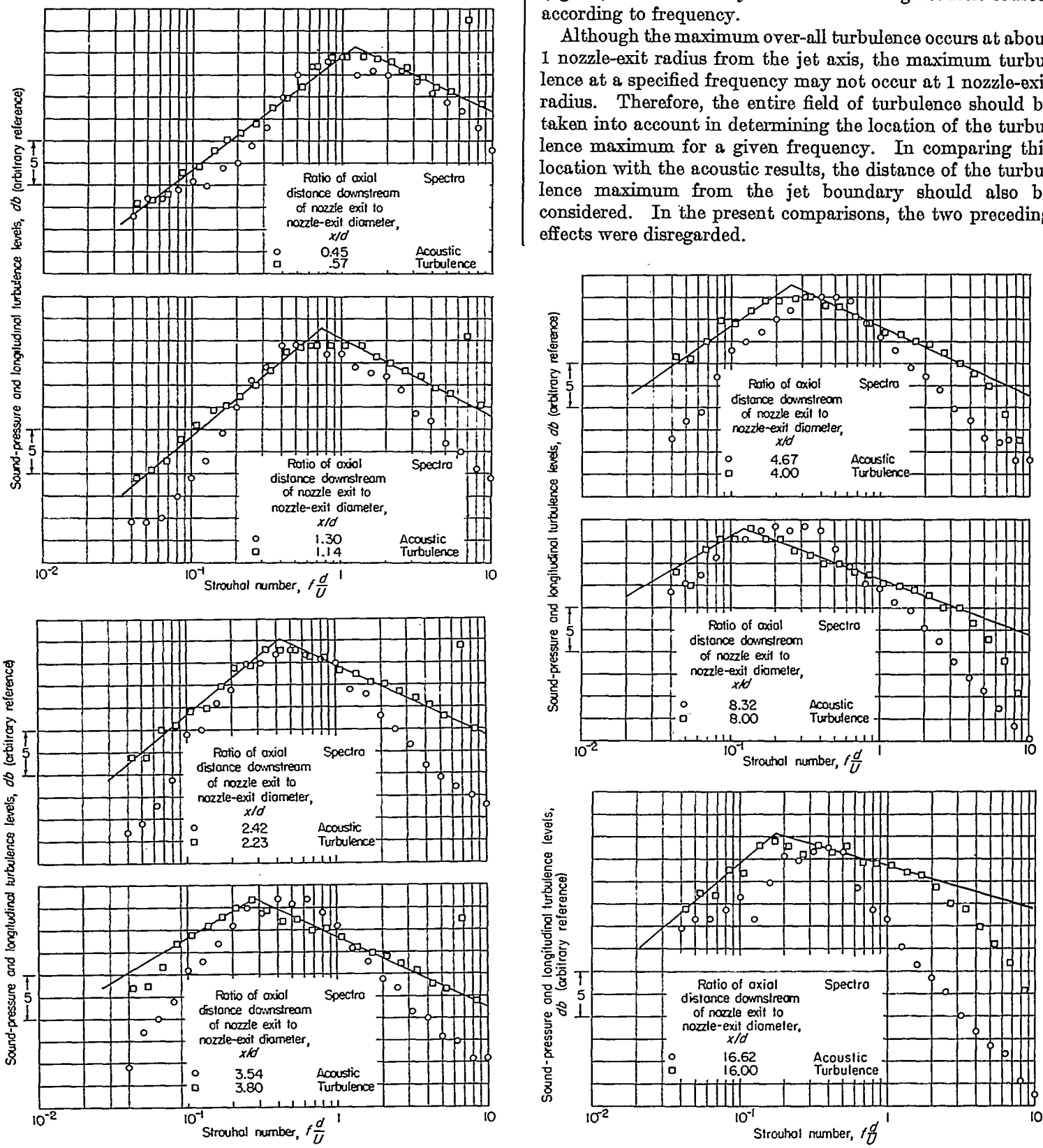

FIGURE 18.—Comparison of jet-engine acoustic spectra along jet boundary with cold-air jet longitudinal turbulent-velocity spectra at 1 jet radius and same dimensionless distance downstream.

CROSS CORRELATION OF SOUND PRESSURES

SOUND-PRESSURE CORRELATION

The characteristics of any noise field are usually given in terms of its time-averaged, that is, statistical, properties such as over-all sound-pressure levels and spectra. These properties are determined by measuring the root-mean-square pressures over the whole frequency range and in frequency bands. The sound pressures created by a jet are random in time, but their time-averaged products may have a spatial relation. The usual properties of root-mean-square pressure and spectra may not be sufficient to define the load on a structure. The loading on a surface is related not only to the root-mean-square pressure at various points, but also to the relative simultaneity of pressure amplitudes acting over the surface. If the pressures act in unison at all points, then the root-mean-square load is simply the product of the root-mean-square pressure and the area of the surface. Usually, however, the instantaneous pressures are not in unison and the relation between the pressures is measured in terms of a statistical relation such as a correlation coefficient.

The correlation coefficient R of any two fluctuating quantities a is defined as

$$R=\frac{\overline{a_1a_2}}{\sqrt{\overline{a_1^2}}\sqrt{\overline{a_2^2}}}$$

where the bars indicate a time average so that

$$\overline{a_1a_2}=\lim_{T\to\infty}\frac{1}{T}\int_0^T a_1(t)a_2(t)\,dt$$

where, for practical purposes, T is a time of much longer duration than the period of the lowest frequency involved. For the case of fluctuating pressures,

$$R=\frac{\overline{p_1p_2}}{\sqrt{\overline{p_1^2}}\sqrt{\overline{p_2^2}}}$$

where p_1 and p_2 are the instantaneous fluctuating pressure at two points.

The value of R is therefore determined by measuring the instantaneous pressures p_1 and p_2 with two microphones, obtaining their time-averaged product, and normalizing with the product of the root-mean-square values of the two pressures. In the special case where the pressures p_1 and p_2 are linearly related (act in unison), then $p_2=kp_1$ and $R=1$. If p_2 is completely unrelated to p_1, the product p_1p_2 has equal probability of being positive or negative and, consequently, the time average of the product will be zero. Therefore, zero correlation is obtained when the relation between p_1 and p_2 is completely random. There are, however, other conditions that yield zero correlation.

The case of the sound pressures generated by a simple source of strength A and frequency ω can be considered. If r_1 and r_2 are the respective distances of the microphones from the source, as shown in the following sketch:

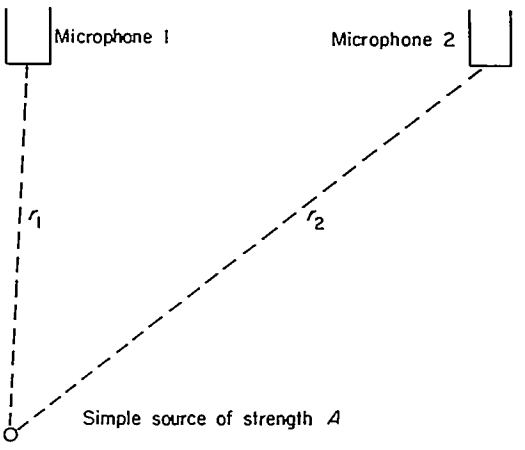

the pressures at 1 and 2 are given as

$$p_1=\frac{A}{r_1}\cos\omega t$$

$$p_2=\frac{A}{r_2}\cos(\omega t+\alpha)$$

The pressures at 1 and 2 are out of phase by angle α, where $\alpha=\omega(r_2-r_1)/c$ and c is the speed of sound in the medium. The averaged product $\overline{p_1p_2}$ is

$$\overline{p_1p_2}=\lim_{T\to\infty}\frac{1}{T}\int_0^T\frac{A^2}{r_1r_2}\cos\omega t\cos(\omega t+\alpha)dt=\frac{A^2}{2r_1r_2}\cos\alpha$$

and

$$\sqrt{\overline{p_1^2}}=\frac{A}{\sqrt{2}r_1}$$

$$\sqrt{\overline{p_2^2}}=\frac{A}{\sqrt{2}r_2}$$

Therefore, the correlation coefficient R between 1 and 2 is $\cos\alpha$. For a single frequency the correlation coefficient and the cosine of the phase angle are equivalent and, hence, can have any value from -1 to 1. There is no real necessity for limiting the previous example to a single source.[1] Any number of sources that produce sinusoidal waves of a single frequency and random strength will induce resulting pressure fluctuations

$$p_1=B_1\cos\omega t$$

and

$$p_2=B_2\cos(\omega t+\beta)$$

at the two microphones. The coefficients B represent the resulting pressure amplitudes at the microphones, and β is a resultant phase angle. The correlation coefficient is then

$$R=\cos\beta$$

where

$$\beta=\tan^{-1}\left(\frac{A_1\sin\alpha_1+A_2\sin\alpha_2+\ldots+A_n\sin\alpha_n}{A_1\cos\alpha_1+A_2\cos\alpha_2+\ldots+A_n\cos\alpha_n}\right)$$

If β is 90°, then $R=0$. Furthermore, it can be shown that, if the pressures at 1 and 2 were of two different frequencies, the correlation would always be zero.

It should be evident that, even if the sound pressures are distributed over a wide frequency range, the pressure

correlation between two points results only from the relation between the identical frequency components at the two points.

If a series of correlations are determined by moving one microphone relative to another, a graph such as shown in figure 19 (a) may be obtained. When the microphones are very close together, the two microphones measure the same pressure and the correlation is unity. As the microphones are separated, the correlation coefficient falls below unity. A useful equivalent to the load on a rigid surface can be determined from the correlation coefficient in the following manner: From the definition of the correlation coefficient, it follows that

$$\overline{p_1 p_2} = R\sqrt{\overline{p_1^2}}\sqrt{\overline{p_2^2}}$$

where all quantities on the right side of the equation are obtainable. The time-averaged quantity $\overline{p_1 p_2}$ is a constant for any given microphone separation. Thus, over the total period T the constant value of $\overline{p_1 p_2}$ is equivalent to the product $P_1 P_2$ of two steady-state pressures P_1 and P_2. If a value is selected for P_1, which may be regarded as the pressure associated with the stationary microphone, then P_2 can be computed from

$$P_2 = R\sqrt{\overline{p_1^2}}\,\frac{\sqrt{\overline{p_2^2}}}{P_1}$$

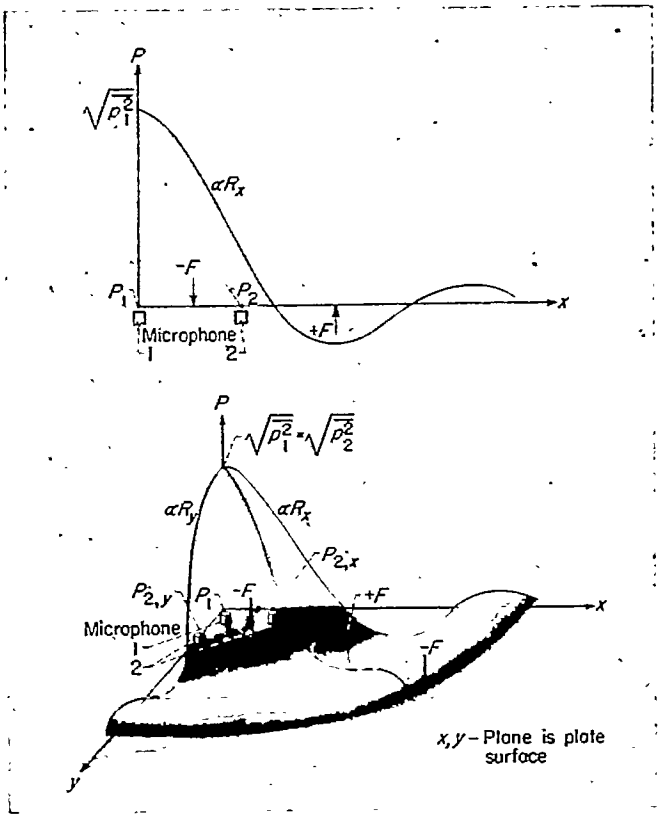

(a) Determined from measurements of R_x.
(b) Determined from measurements of R_x or R_y.

FIGURE 19.—Steady-state pressure distributions indicated by correlation measurements. Arrow with F indicates instantaneous direction of applied force.

where, by virtue of R, P_2 is a function of the microphone separation. Because $R=1$ when the microphone separation is zero, $P_1=\sqrt{\overline{p_1^2}}$ and $P_2=\sqrt{\overline{p_2^2}}=\sqrt{\overline{p_1^2}}$. When the microphones are separated, $P_1=\sqrt{\overline{p_1^2}}$, as before, but $P_2=R\sqrt{\overline{p_2^2}}$ where P_2 is the most probable value of p_2 corresponding to $P_1=\sqrt{\overline{p_1^2}}$. The last four equations permit computation of a time-average pressure distribution along a line connecting the microphones, when the sound pressure at the stationary microphone is $P_1=\sqrt{\overline{p_1^2}}$. The result amounts to replacing the random pressure distribution along the line of microphone separation by an equivalent steady-state distribution, as shown in figure 19 (a).

In order to obtain a measure of the force distribution over a surface area, it is necessary to measure correlations in both the lateral and longitudinal directions (y- and x-directions, respectively, fig. 20). From such measurements, the area distribution of the pressures can be approximated in the manner shown in figure 19 (b). In this figure, curves of constant P_2 have been assumed to be ellipses in planes parallel to the x, y-plane. By using such a distribution, it is possible to calculate an effective instantaneous force distribution on the plate. Before such a concept has any value, however, it must be associated with some frequency; that is, the pressure variation with time must be known.

The fluctuating pressure field near a jet is of an extremely complex character since, at any point in the field, the pressure results from a space distribution of randomly fluctuating sources. Furthermore each source produces a fairly wide range of frequencies. However, the wave form of the sound at any point results from the cumulative effect of all the sources. The usual wave form in the near field of a jet has a random amplitude and a fairly peaked frequency distribution. The largest contribution to the over-all sound-pressure correlation will result from the energy centered around this peak. To a first approximation, therefore, the loading distribution of the over-all pressures previously described might be assumed to fluctuate harmonically with a frequency corresponding to the peak frequency of the spectrum.

Surfaces in aircraft are usually resonant and would normally be expected to fail most rapidly if excited by pressure fluctations in the band of resonant frequencies. Thus, the pressure correlations of interest in many cases are those associated with a narrow band of frequencies. The data reported herein have, therefore, been analyzed in approximately ½-octave bands. For comparison with the ½-octave analyses, the correlation coefficient was also determined for a narrow band width (12 cps) with a midfrequency of 500 cps.

In order to determine the fatigue of a resonant panel, the panel should be loaded with a harmonically fluctuating load corresponding to the resonant frequency band. The amplitude of the load over the surface would be determined from the correlation curve for the band of interest and the root-mean-square pressure (in the same band). The procedure would be the same as described previously for over-all sound pressures but limited to the band width for which the panel is resonant.

The practical determination of the correlation coefficient for this investigation was obtained by the following method: The output voltage e of a microphone is linearly related to the fluctuating pressures for the range of frequencies and pressures of interest; so

$$p_1=k_1e_1$$

and

$$p_2=k_2e_2$$

and, therefore,

$$R=\frac{\overline{e_1e_2}}{\sqrt{\overline{e_1^2}}\sqrt{\overline{e_2^2}}}$$

The correlation coefficient of sound pressures at two points in space is therefore obtained in exactly the same manner as the correlation coefficient for two fluctuating velocities in turbulence measurements (refs. 20 and 15). It is therefore possible to obtain correlation coefficients quite simply with a correlation computer of the type discussed in reference 15 and described in detail in appendix B of this report.

APPARATUS AND PROCEDURE

The equipment required for the determination of the space correlation of the acoustic pressures near the jet can best be described in three parts: (1) the engine and its associated equipment, (2) the equipment for obtaining and recording the acoustic data, and (3) the correlation equipment. The first two items and their use will be described in the succeeding paragraphs together with a partial description of the correlation equipment and its use. The correlation computer is described in appendix B.

ENGINE

The engine used for the investigation is shown in figure 1. For the tests to be described, the exhaust nozzle exit was 22¼ inches in diameter. The pressure ratio across the nozzle under test-stand conditions when the engine was operated near rated power was approximately 2.2, resulting in choked flow at the nozzle and expansion to slightly supersonic flow just downstream of the nozzle. The engine was mounted in the outdoor thrust stand shown in figure 1. Engine operating conditions were chosen that would allow duplication of the engine thrust condition over the range of atmospheric conditions expected to prevail during the experiments. In addition, the time required to obtain the correlation data limited the engine operation to somewhat less than full power. All the data presented herein, unless otherwise indicated, were obtained at a thrust of approximately 9600 pounds and a jet velocity (ratio of thrust to mass flow) of 1850 feet per second. The afterburner was not used for this investigation.

Measuring stations were set up outside the jet-temperature and total-pressure (velocity) boundaries (fig. 4) determined for conditions of little or no wind. The measuring stations are shown in figure 20.

ACOUSTICAL EQUIPMENT

In order to obtain the space correlation data, it was necessary to provide a means for simultaneously recording the signals from two microphones precisely located in the sound field.

Microphone positioning.—The remotely controlled and remotely indicating microphone-positioning device shown in figure 3 was used to provide the microphone movement required. One of the microphones was mounted in a fixed position to the body of the device and the other was mounted on a movable carriage. The whole assembly could be positioned at any point in the sound field outside the jet. Positioning of the fixed microphone and the traversing mechanism was accomplished by measurement from permanent markers. Later in the investigation the traversing mechanism was modified to provide motion in the vertical direction.

At the beginning of each experiment, the two microphones were horizontal and adjacent with the microphone faces in the same vertical plane and at the engine centerline height. For the correlation data taken along the jet boundary (x_1-direction), this vertical plane, the a, b, c, d-plane in figure 20,

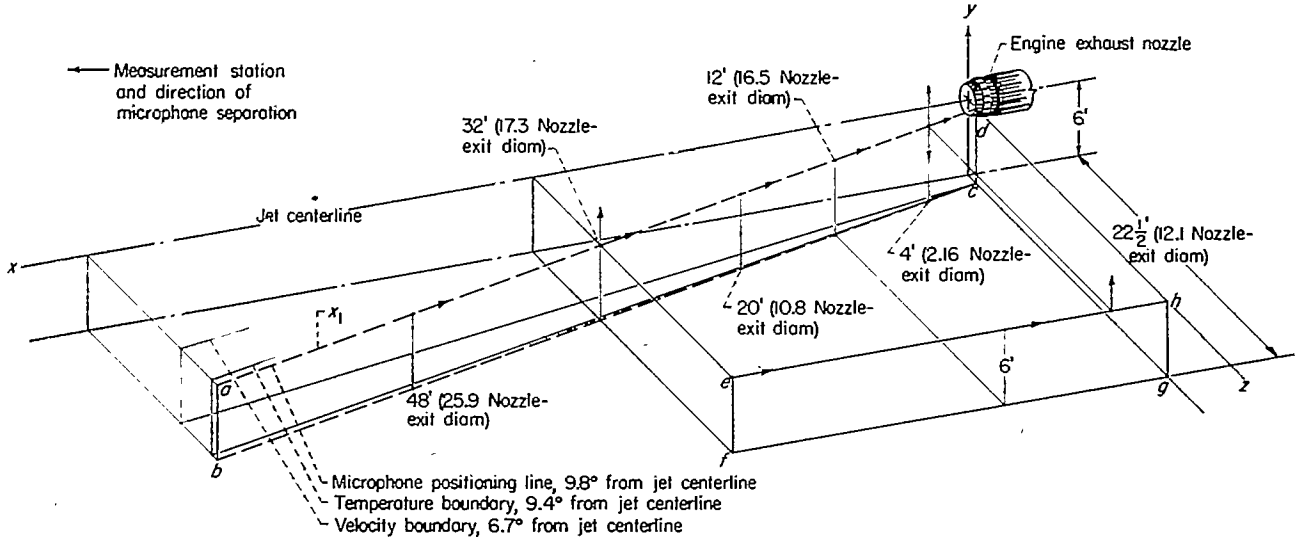

FIGURE 20.—Location of jet boundaries and measurement stations.

was along the microphone location line. Correlation data were also obtained at three locations away from the jet boundary with the plane of the microphone faces parallel to the jet centerline (x-direction) and in the e, f, g, h-plane. For the longitudinal correlations, one microphone was moved in a horizontal direction away from the fixed microphone and toward the engine. For the lateral correlations, the microphone was moved upward from the engine centerline height.

With the microphones adjacent, the microphone centers were approximately 1 inch apart. Magnetic tape records of several minutes duration were made with the microphones adjacent for purposes of calibration of the correlation computer. The microphones were then separated in small increments and tape records of approximately 1-minute duration were taken at each position. Small increments were taken at first, and then larger increments were used when the total separation was several feet.

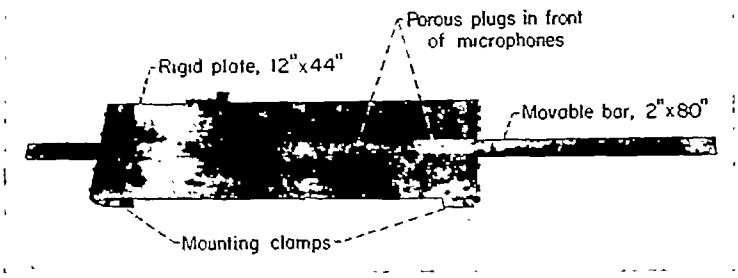

FIGURE 21.—Plate used for determining sound-pressure correlation on surface.

For the study of the longitudinal correlation over the surface of a panel, a stiff aluminum plate consisting of three segments was used as shown in figure 21. The center segment was a sliding bar approximately twice the length of the fixed top and bottom sections. The microphones were mounted behind porous, sintered stainless-steel plugs flush with the plate surface to protect the microphones. These plugs do not affect sound pressures for the range of frequencies of interest. The movable microphone was mounted near the center of the bar and the fixed microphone in the adjacent plate. The actuating and position-indicating mechanism was similar to that previously described. The plate was mounted on vertical stands at the engine centerline height. The face of the plate was in a vertical plane along the microphone location line near the jet boundary.

Microphones.—Small condenser microphones of approximately ⅝-inch diameter were used to obtain both the free-field and plate data. Because of the differences in sound level existing at the various measuring stations, it was necessary to use several sets of microphones having appropriate sensitivities to avoid amplitude distortion of the signals. The signals from the microphones were transmitted by compensated cable systems to the recording station located in the small engine-control building (fig. 3).

Data recording.—The signals from the two microphones were recorded simultaneously on a single tape by a dual-channel magnetic-tape recorder. The signal strengths from the microphone systems were recorded at equal amplitudes by controlling the recording levels separately. A cathode-ray oscilloscope was used to monitor the input signals to the recorder. From observation of the Lissajou's figures formed using both input signals simultaneously, a rough estimate of the degree to which the signals were correlated was possible during the progress of the experiments.

Data processing.—In order to determine the correlation of the data, the tapes were run through the tape-handling playback portion of the correlator described in the appendix. The dual-channel pickup heads were adjusted so that they picked up signals recorded at the same time. The correlation coefficient was then determined for each microphone separation at all the measuring stations and engine power conditions studied. These values of the correlation coefficient are overall values for the entire frequency range of the microphone signals. Correlation of frequency-band filtered signals was also obtained. From the playback pickup system, the signals were passed through high-pass and low-pass electronic variable-frequency filters and then to the correlation computer. The frequency cutoff of the filters had a slope of 20 decibels per octave. The band width measured to the frequencies of 3-decibel attenuation for all of the frequency bands investigated is shown in the following table:

Midfrequency, cps	Frequency at 3-db attenuation, cps		Band width, cps
	Low	High	
100	80	119	39
200	161	242	81
300	244	360	116
400	326	486	160
500	405	600	195
600	485	710	225
800	650	960	310
1000	800	1200	400

In addition, one set of narrow-band filters was made that had a band-pass width of 12 cps at the 3-decibel attenuation point and a midfrequency of 500 cps.

The limitation of the frequency bands shown (100 to 1000 cps) in the preceding table results from the frequency distribution of the sound and the limit on the maximum possible signal (voltage) level that can be impressed on the tape. The peak of the frequency spectrum occurs between 100 and 1000 cps for all the acoustic near field. For most positions the spectrum peak occurs near 500 cps. The available signal in each band drops off quite sharply on either side of the spectrum peak, and for most cases bands above 1000 and below 100 cps do not contain a sufficient signal for a reasonably accurate value of correlation with the computer described in appendix B. This, however, should not be particularly important since the sound pressures outside the 100- to 1000-cps region are far below the peak values and probably would not have sufficient energy to affect the aircraft structure.

It would, of course, be possible to filter the microphone signal in frequency bands ahead of the recorder and, hence, obtain data over a much wider frequency range. This would result in an exceedingly large amount of engine operation time and, therefore, was not considered.

RESULTS AND DISCUSSION

The results presented herein are largely confined to the effect of various parameters, such as jet velocity and measurement position, on the correlation coefficient. All the correlation figures presented have correlation coefficient as the ordinate and a dimensionless microphone separation (ratio of microphone separation to nozzle-exit diam. s/d) as the abscissa. The data presented were obtained both longitudinally (x- or x_1-direction) and laterally (y-direction). The x_1-direction is measured along the jet boundary and is at an angle of 9.8° to the x-, or axial, direction (fig. 20).

LONGITUDINAL CORRELATION

A typical set of correlation data is shown in figure 22. These data were obtained at a position approximately 17.3 nozzle-exit diameters downstream (measured along the jet boundary) of the engine and 12.1 nozzle-exit diameters from the jet centerline. Correlations are shown for the over-all sound pressure and for sound pressures in various frequency bands with midfrequencies from 100 to 1000 cps. The width of each band and its midfrequency is tabulated in the APPARATUS AND PROCEDURE section.

The correlation curves of figure 22 show interesting characteristics. There is a definite order to the results. The microphone separation for which the correlation coefficient is initially zero occurs at decreasing s/d values, and the curves sharply steepen with increase in frequency. The separations for maximum negative correlations and the second zero-correlations follow this same trend. The maximum negative correlation values show a definite tendency to increase (negatively) to a midfrequency of 400 cps and to decrease thereafter.

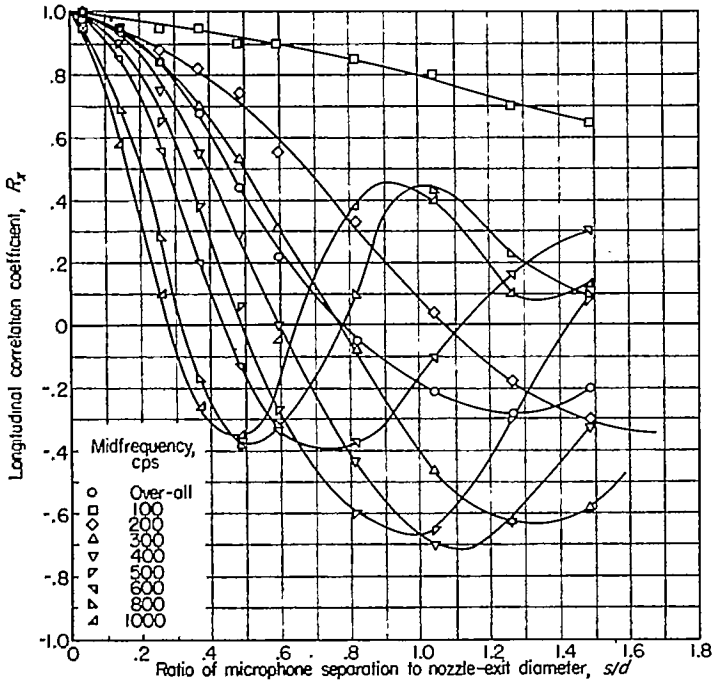

FIGURE 22.—Longitudinal sound-pressure correlation in various frequency bands. Distance downstream of nozzle exit, x_1, 17.3 nozzle-exit diameters; distance from jet centerline, z, 12.1 nozzle-exit diameters.

For the data shown in figure 22, the peak of the frequency spectrum occurs between 300 and 400 cps. The over-all correlation curve also falls between the 300- and 400-cps midfrequency correlation curves. All the correlation data exhibited this characteristic; that is, the over-all correlation curve fell near the correlation curves corresponding to the peak of the spectrum. The approximation of the over-all curve by a curve of single frequency as described previously in the section SOUND-PRESSURE CORRELATION would appear to be useful for structural loading purposes.

Effect of jet velocity.—The over-all sound-pressure correlation for a range of jet velocities from 630 to 1780 feet per second is shown in figure 23. These data were obtained along the jet boundary 2.16 nozzle-exit diameters downstream of the nozzle exit. In general, the shapes of the curves are nearly the same, and the effect of jet velocity appears to be quite small.

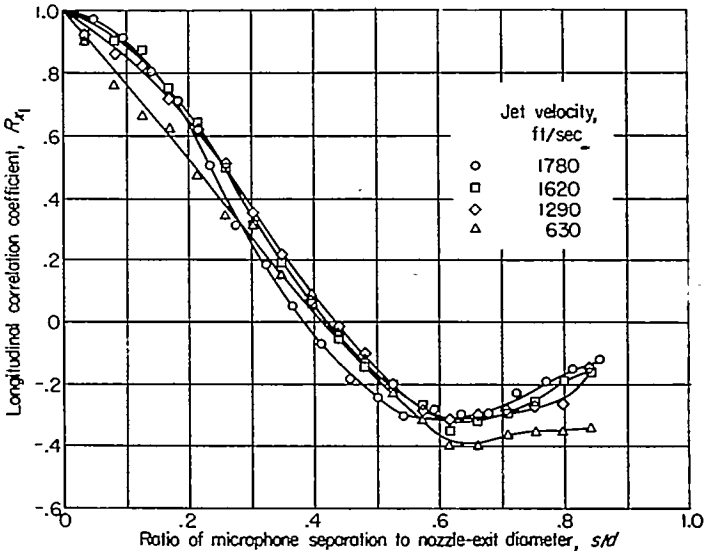

FIGURE 23.—Longitudinal correlation along jet boundary of over-all sound pressure for range of jet velocities. Distance downstream of nozzle exit, x_1, 2.16 nozzle-exit diameters.

The small effect of velocity might well be inferred from the results of reference 15, which show very little effect of exit velocity on the scale and intensity of turbulence. Since the sound-pressure spectrum near the jet is quite similar to the turbulent velocity spectrum in the jet, it would be expected that the near-field sound would reflect the same trends as the turbulence results.

The effect of velocity on the correlation coefficient for several frequency band widths is shown in figure 24. As might be expected from the previously discussed results on the over-all sound-pressure correlation, the effect of velocity on the correlation for the various band widths is quite small.

Effect of position.—The correlation of the over-all sound pressures at various positions along the jet boundary is shown in figure 25. Near the nozzle exit, 2.16 nozzle-exit diameters downstream along the boundary, the region of positive correlation extends to an s/d value of 0.385. Farther downstream the region of positive correlation increases, but at 6.5, 10.8, and 17.3 nozzle-exit diameters the region of positive correlation is nearly the same and appears to give a first zero crossing at about s/d of 0.93. The correlation of these same data for the various frequency bands is shown in figure 26. In general, the correlations of figure 26 follow the general trend of decreasing region of positive correlation with increasing frequency, as discussed previously (fig. 22). This is shown quite clearly in figure 27, where the initial zero-crossing point (fig. 26) is plotted as a function of frequency. The straight line relation of the data indicates that the distance for initial zero crossing is related to the frequency by an equation of the form

$$s/d=\frac{k}{(\text{frequency})^n}$$

The value of n appears to increase nonuniformly from about 0.5 near the nozzle to about 1.2 far downstream.

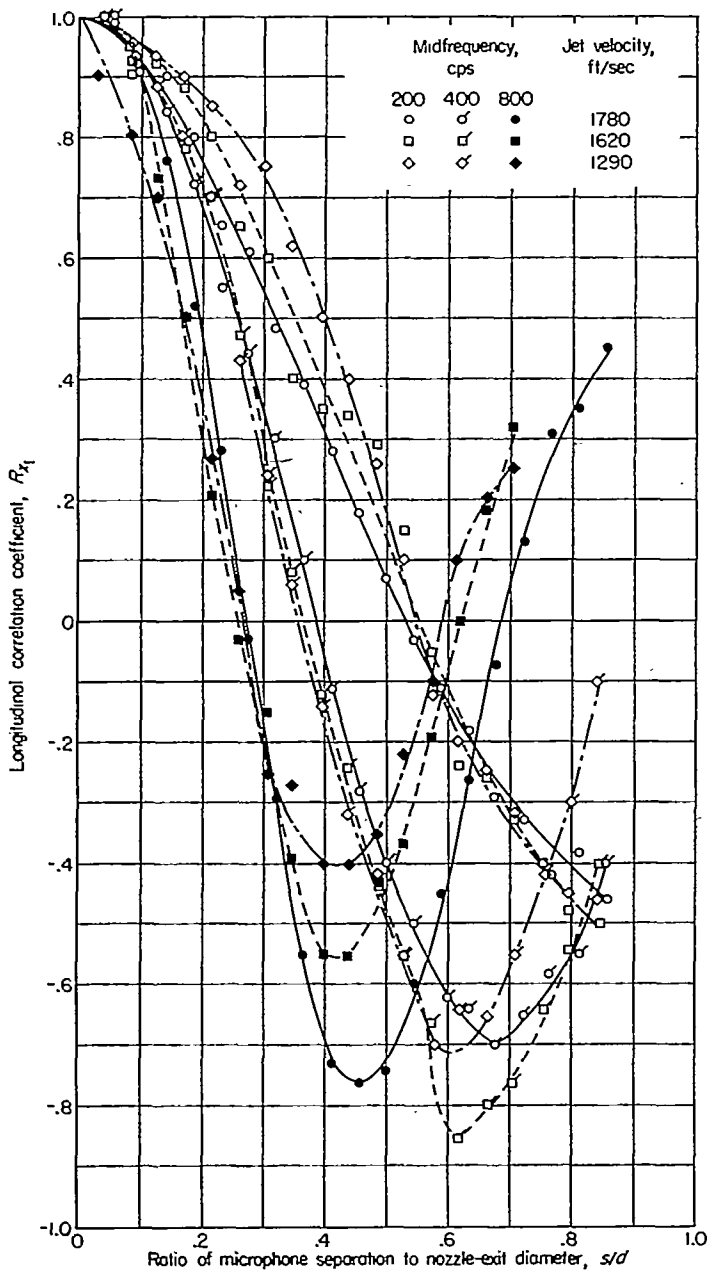

FIGURE 24.—Longitudinal correlation of sound pressure for three frequency bands. Distance downstream of nozzle exit, x_1, 2.16 nozzle-exit diameters.

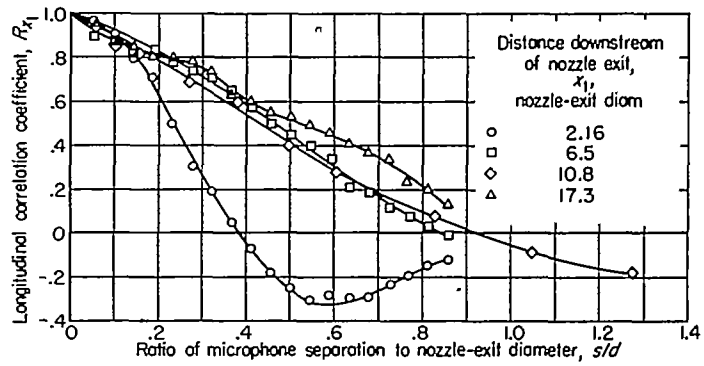

FIGURE 25.—Longitudinal correlation of over-all sound pressure at several locations along the jet boundary.

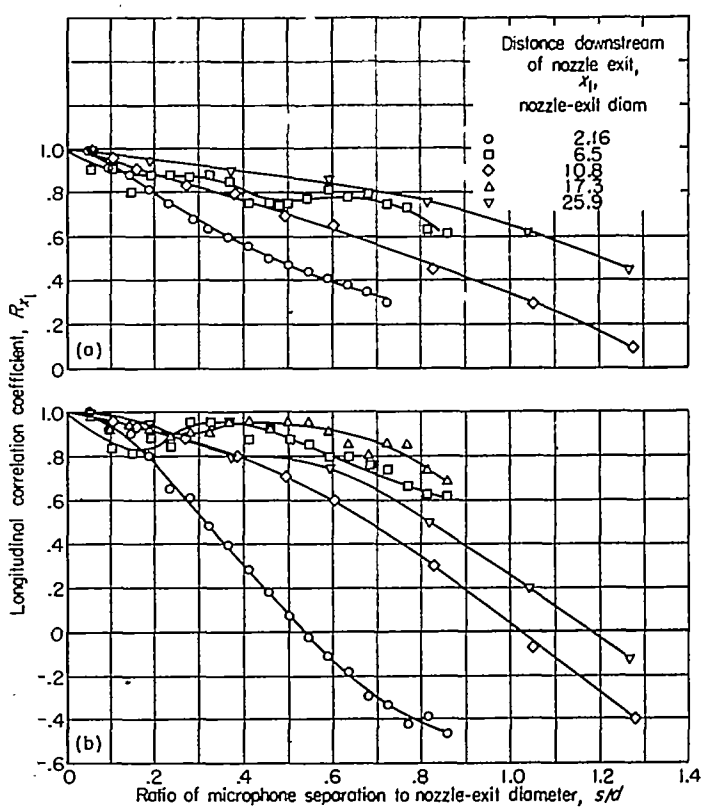

(a) Midfrequency, 100 cps.
(b) Midfrequency, 200 cps.

FIGURE 26.—Longitudinal correlation of sound pressure in various frequency bands for several positions along the jet boundary.

The results shown in figure 26, however, do not show exactly the same order as the correlations of over-all sound pressures in figure 25. This should be expected since the spectrum distribution of the sound changes in moving downstream from the nozzle exit. The peak of the sound-pressure spectrum occurs at decreasing frequency with increasing downstream distance. Because correlations result from Fourier transforms of spectra, it should be expected, therefore, that the shift in the spectrum would show up in the band-pass correlations.

In figure 28 is shown a comparison of over-all sound-pressure correlations measured on the jet boundary and 12.1 nozzle-exit diameters from the jet centerline for two downstream distances. At a downstream distance of 6.5 nozzle-exit diameters, the shape of the correlation curves are vastly different. On the boundary, the first zero-correlation position occurs at an s/d value near 0.85, whereas 12.1 nozzle-exit diameters from the jet the correlation coefficient appears to approach zero asymptotically. At 17.3 nozzle-exit diameters downstream of the nozzle exit, the curves are somewhat similar, although the microphone separation at the first zero crossing is slightly larger near the jet. The data of figure 28 in the various bands are also shown in figures 22 and 26 except for the position 6.5 nozzle-exit diameters downstream of the nozzle exit and 12.1 nozzle-exit diameters from the centerline. These correlations are presented in figure 29.

Effect of band width.—The correlation of sound pressures would ideally be made for a band width corresponding to the band width to which the surface is responsive. This may not be necessary, as illustrated in figure 30. In this figure, data at several locations in the field are presented for two band widths, 195 and 12 cps, both having essentially the same midfrequency (500 cps). It is evident that the initial region of positive correlation is practically independent of the width of the band pass for a band pass less than 1 octave. There is a tendency when reducing the band width for an increase in the maximum negative value of the correlation coefficient but little effect on the positions where the values of first zero crossing occur. The small effect of decreasing the band width from 195 to 12 cps indicates that further decreases in the band-pass width would show only an increase in the absolute magnitude of the second maximum positive and negative values but little change in the zero-crossing positions. This result agrees with a similar treatment of turbulence data (ref. 15). It should be obvious that increasing the band width by an appreciable amount is bound to shift the curves toward the over-all sound-pressure correlation.

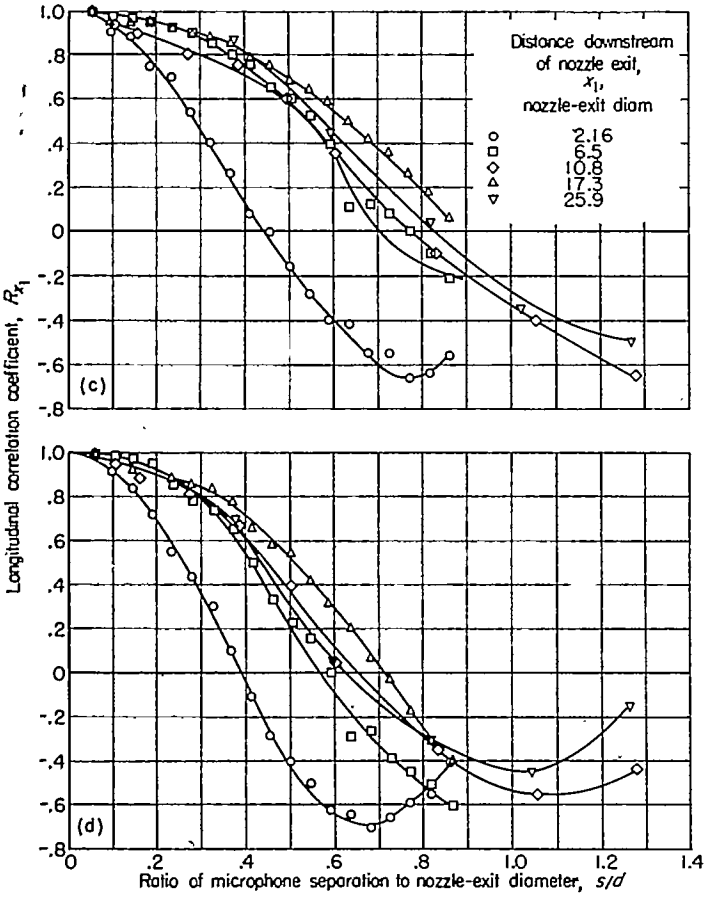

(c) Midfrequency, 300 cps.
(d) Midfrequency, 400 cps.

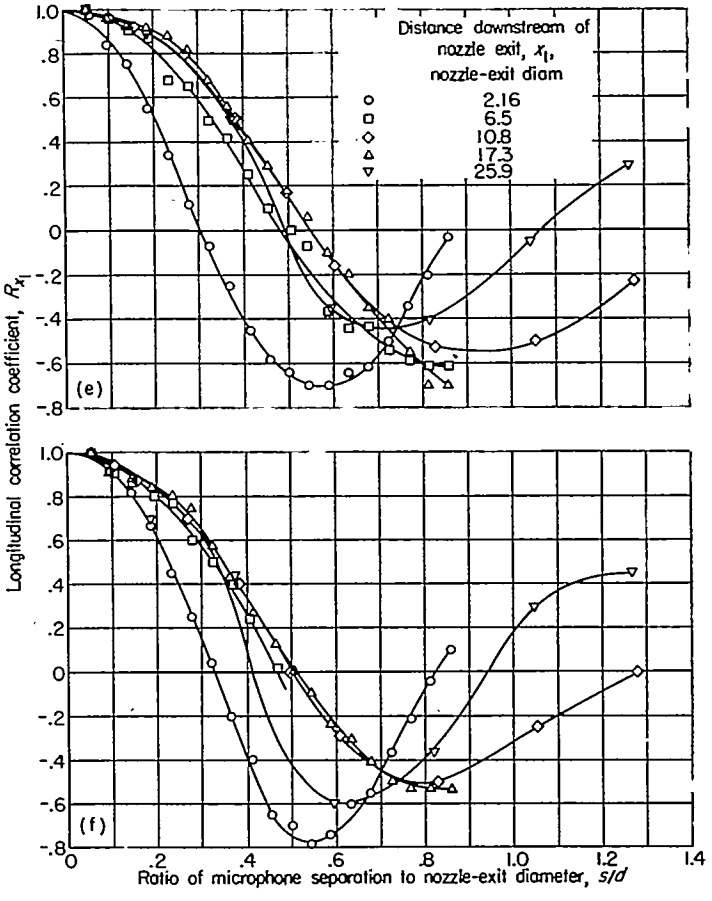

(e) Midfrequency, 500 cps.
(f) Midfrequency, 600 cps.

FIGURE 26.—Continued.

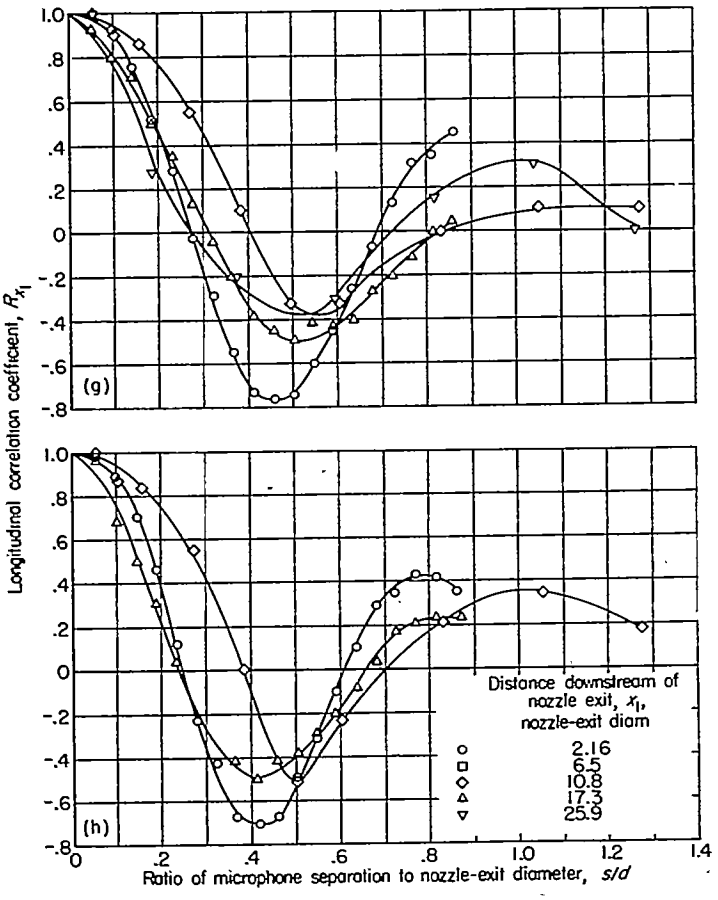

(g) Midfrequency, 800 cps.
(h) Midfrequency, 1000 cps.

FIGURE 26.—Concluded.

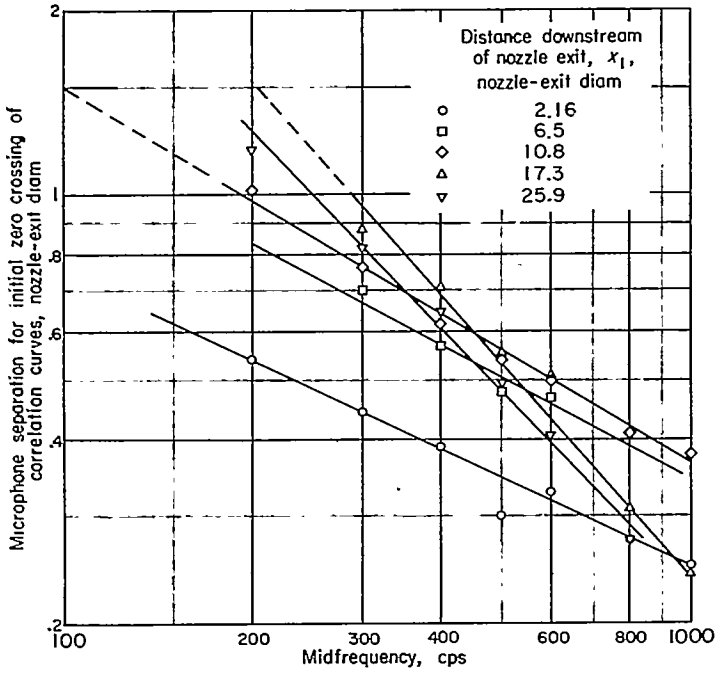

FIGURE 27.—Initial zero crossing of longitudinal correlation curves as function of frequency.

Comparison of free field and plate.—The results presented thus far have been concerned with the correlation in free field. A point of considerable interest is the relation between

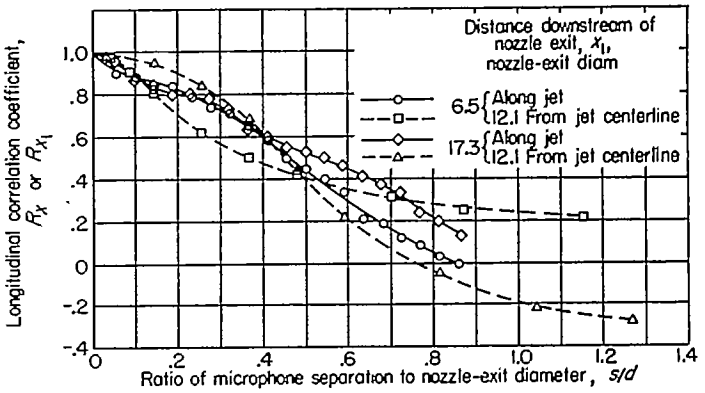

FIGURE 28.—Longitudinal correlations of over-all sound pressure along jet boundary and 12.1 nozzle-exit diameters from jet center-for two distances downstream of nozzle exit.

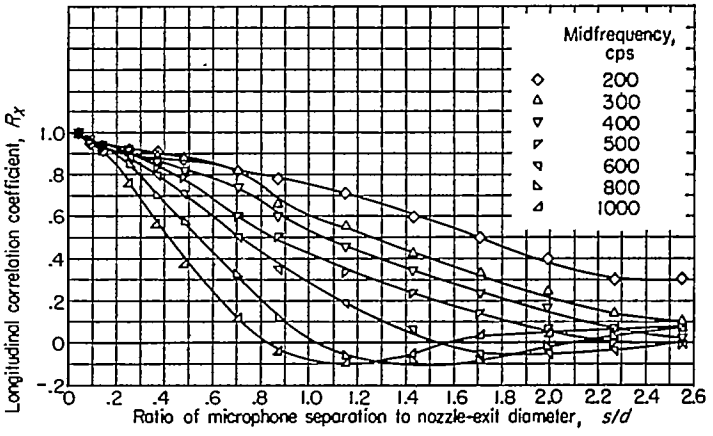

FIGURE 29.—Longitudinal correlation of sound pressure for several frequency bands. Distance downstream of nozzle exit, x_1, 6.5 nozzle-exit diameters; distance from jet centerline, z, 12.1 nozzle-exit diameters.

a free-field correlation and a correlation on a surface. It might be expected that the introduction of a surface into a sound field would cause some change in the correlation.

As a preliminary estimate of this effect, a single set of data was obtained of the correlation on a flat plate. The dimensions of the plate and the microphone locations are shown in figure 21. The data were obtained with the fixed microphone located approximately 2.7 nozzle-exit diameters downstream of the nozzle exit, the long dimension of the plate along the jet boundary, and with the plate surface tangent to the jet. From figure 25 it can be seen that the free-field over-all sound-pressure correlation is much smaller than the physical dimensions of the plate; that is, the correlation has become nearly zero in the first 0.9 nozzle-exit diameter compared with the plate length of 1.98 nozzle-exit diameters.

The over-all sound-pressure correlation coefficient for both the plate and free field at approximately the same spatial location is shown in figure 31. Also shown in the figure are the results for several frequency bands. From these data it can be seen that the surface correlation and the free-field correlation for each frequency are not too different. The correlation curves for the plate have slightly different shapes and greater negative values than the free-field results. This might well be caused by the slightly different locations of

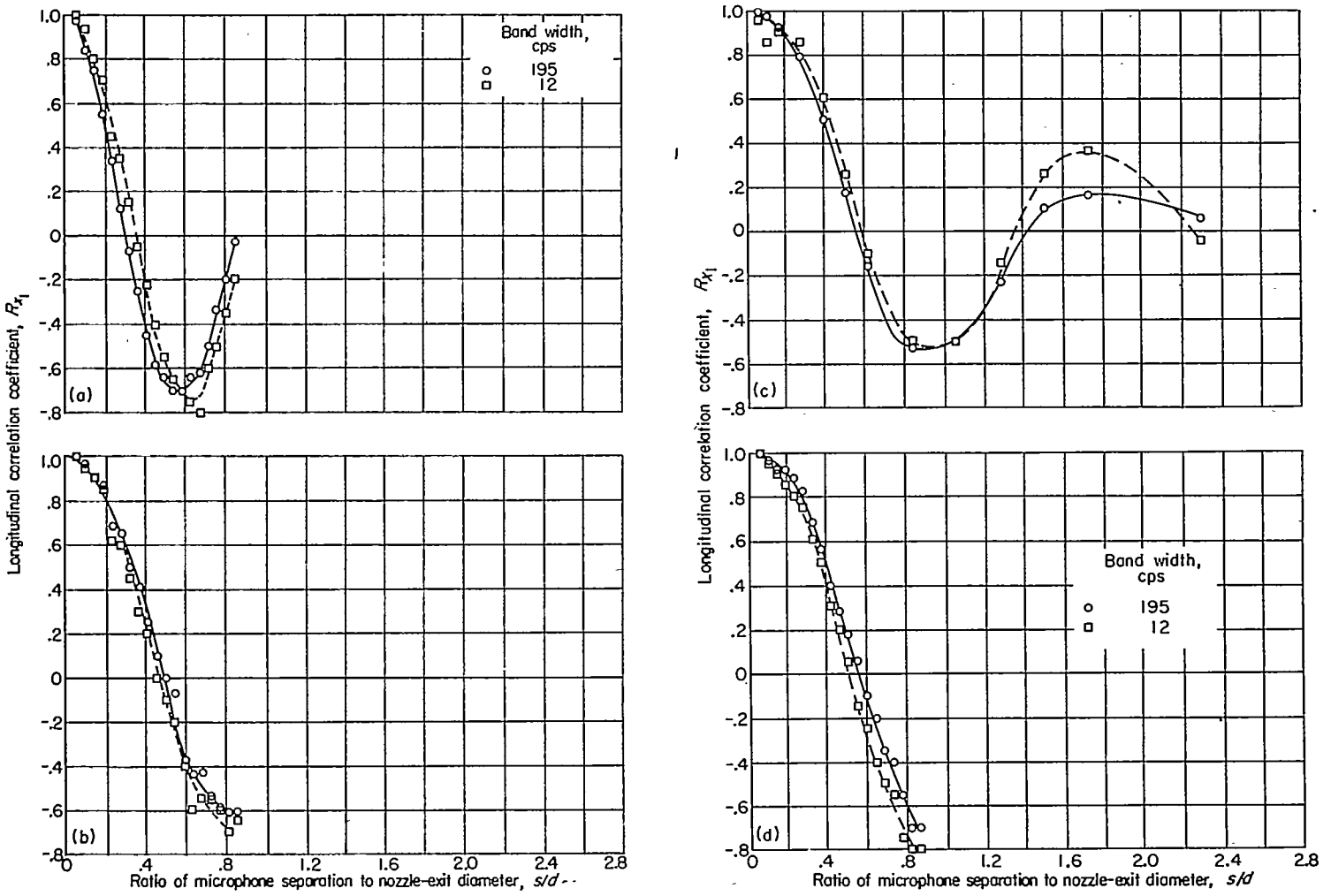

(a) Distance downstream of nozzle exit, x_1, 2.16 nozzle-exit diameters.
(b) Distance downstream of nozzle exit, x_1, 6.5 nozzle-exit diameters.
(c) Distance downstream of nozzle exit, x_1, 10.8 nozzle-exit diameters.
(d) Distance downstream of nozzle exit, x_1, 17.3 nozzle-exit diameters.

FIGURE 30.—Longitudinal correlations of sound pressure for two band widths having midfrequencies of 500 cps.

the plate and free-space measurements. The plate location (fixed microphone) was approximately 1 foot downstream of the free-field measurements. It would appear, therefore, that correlation is relatively unaffected by the presence of the body in the field, at least for the case where the body is larger than the area over which the pressures are correlated to a large degree.

It is interesting to note that the actual sound-pressure levels on the plate (when placed along the jet boundary) are much higher than those measured in the free field.

LATERAL CORRELATION

In general, it would be expected that a sound-pressure correlation would involve a spatial volume. That is, a constant value of the correlation coefficient would have a shape in space in the same sense that a turbulence correlation has in a jet (ref. 15). For structural considerations, it is necessary to know the correlation in the plane of the surface under consideration. Measurements have therefore been made along a vertical line (y-direction, fig. 20) at several positions corresponding to measurement points of longitudinal correlation. No measurements were made in the direction normal to the plane of the longitudinal and lateral correlations.

Effect of position.—Correlations of the over-all sound pressures at three positions are shown in figure 32. In each case the fixed microphone was held in the horizontal plane of the jet centerline (fig. 20) and the movable microphone was moved vertically upward.

It is apparent from the figure that the pressures are correlated over a considerable distance. In fact, only the data at 2.16 nozzle-exit diameters downstream along the jet boundary show a zero correlation within the actuator limits. If the data of figure 32 are compared with the longitudinal correlations for the two comparable space positions (fig. 25), it is apparent that the lateral distance to the first zero crossing is larger than the longitudinal.

A single set of measurements moving the microphone vertically downward were made at 2.16 nozzle-exit diameters downstream along the jet boundary. These data were nearly identical to the results obtained when moving the microphone upward.

Correlation in frequency bands.—The correlation in frequency bands at 17.3 nozzle-exit diameters downstream is shown in figure 33. These data show exactly the same trends as the longitudinal correlations in frequency bands (fig. 22).

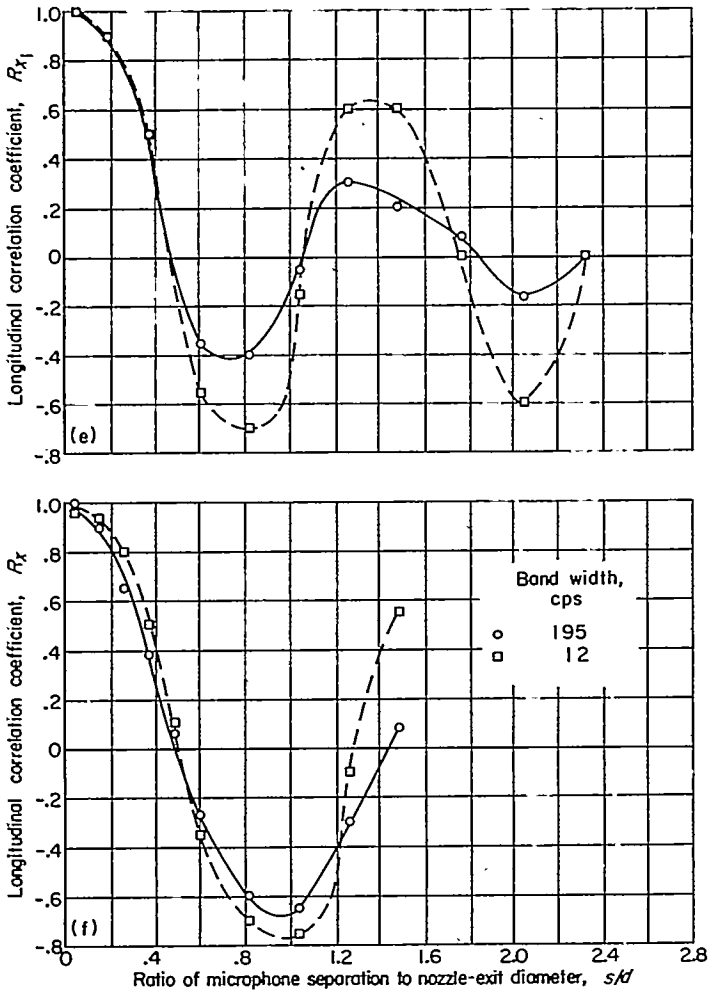

(e) Distance downstream of nozzle exit, x_1, 25.9 nozzle-exit, x_1 diameters.

(f) Distance downstream of nozzle exit, x_1, 17.3 nozzle-exit diameters; distance from jet centerline, z, 12.1 nozzle-exit diameters.

FIGURE 30.—Concluded.

Effect of band width.—The effect of band-pass width on the correlation for two frequency bands at two downstream distances is shown in figure 34. It is apparent that the effect of band-pass width is quite small in the initial positive region. The maximum negative value is greater for the narrower pass band, which agrees with the effect on longitudinal correlations presented in figure 30.

CONCLUSIONS

Acoustic measurements in the vicinity of the exhaust of a 10,000-pound-static-thrust turbojet engine indicated that:

1. Maximum over-all quasi-peak sound pressures were of the order of 42 pounds per square foot without afterburning or 63 pounds per square foot with afterburning. These pressures correspond to sound-pressure levels of 160 and 163.5 decibels, respectively. Maximum sound pressures were obtained along the jet boundary immediately downstream of the jet nozzle exit.

2. Maximum sound pressures of the order of 13 pounds per square foot occurred (without afterburning) in each of the three ⅓-octave bands contained in the frequency interval from 350 to 700 cps.

3. Sound-pressure levels at the surface of a stiff plate placed along the jet boundary were greater than the corresponding free-field values.

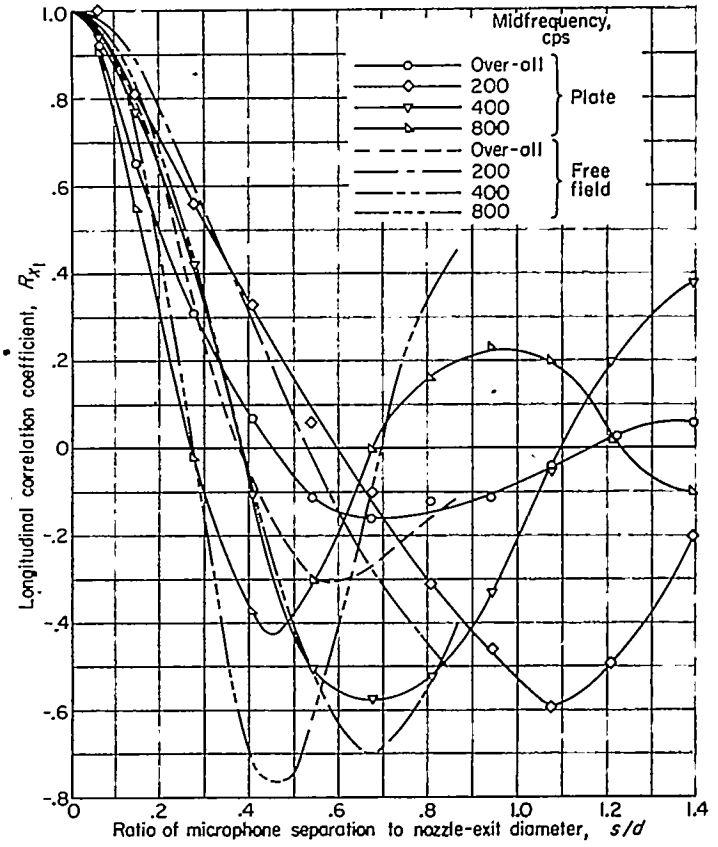

FIGURE 31.—Comparison of longitudinal correlations along jet boundary obtained on plate and in free field for several frequency bands. Fixed microphone, distance downstream of nozzle exit: plate, x_1, 2.7 nozzle-exit diameters; free field, x_1, 2.16 nozzle-exit diameters.

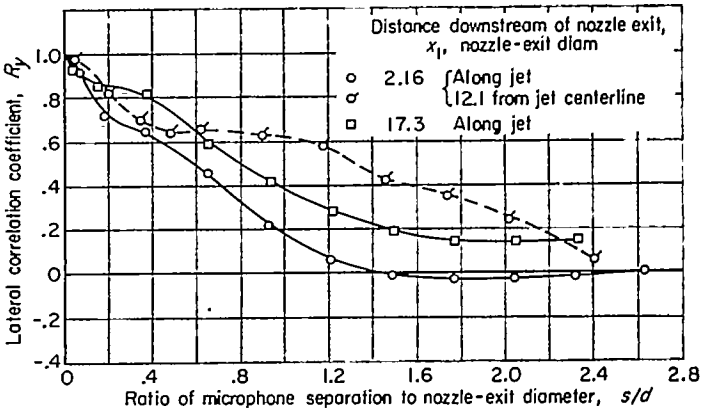

FIGURE 32.—Lateral correlations of over-all sound pressure at several locations in sound field.

4. Throughout most of the length of the jet-mixing region, the distribution according to frequency of acoustic sources was given by

$$\frac{fd}{U}=\left(1.25\,\frac{x}{d}\right)^{-1.22}$$

5. Throughout the length of the mixing region, the relation between spectrum peak frequency and distance downstream was given by $f=(5.6\times10^{-7}x)^{-0.48}$.

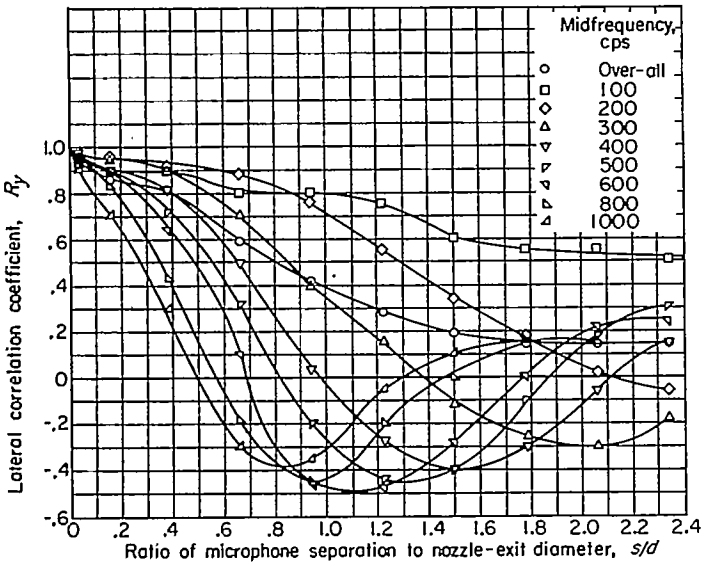

FIGURE 33.—Lateral correlations of sound pressure at jet boundary for various frequency bands. Distance downstream of nozzle exit, x_1, 17.3 nozzle-exit diameters.

By comparing the acoustic measurements for the engine with turbulence measurements for a cold-air jet, the following additional conclusions appear valid:

1. Peak longitudinal turbulent velocities and peak acoustic pressures associated with the same Strouhal number occur at approximately the same dimensionless distance along a jet.

2. Peak longitudinal turbulent velocities and peak acoustic pressures at approximately the same dimensionless distance along a jet possess the same Strouhal number.

3. The distribution according to frequency of acoustic sources along the hot exhaust of a jet engine is similar to that along a cold-air jet. The effect of jet temperature upon the distribution appears to be small or negligible. The rate of expansion of the jet-mixing region may affect the distribution.

4. Acoustic spectra adjacent to a jet-engine exhaust are similar to, but not as flat as, longitudinal turbulent-velocity spectra at 1 nozzle-exit radius and at a similar distance along an air jet.

5. Acoustic and turbulent-velocity frequencies corresponding to values of Strouhal number larger than 0.15 are generated primarily in the jet-mixing region upstream of the tip of the jet core.

The preceding conclusions resulted when the acoustic and turbulence data were compared in terms of distance downstream in jet-nozzle-exit diameters and Strouhal number based on jet-nozzle-exit diameter and the jet bulk velocity.

As part of the study of the near noise field of a jet exhaust, the space correlations of the sound pressures have been measured and the following results obtained:

1. The size of the region of positive longitudinal correlation of the over-all pressures along the jet boundary (the distance to the first zero crossing of the correlation curves) varied from 0.385 to 0.93 nozzle-exit diameters.

2. Longitudianal correlation curves obtained over a range of jet velocities from 630 to 1730 feet per second showed, in general, little change in the over-all and frequency bandwidth correlations as a function of jet velocity.

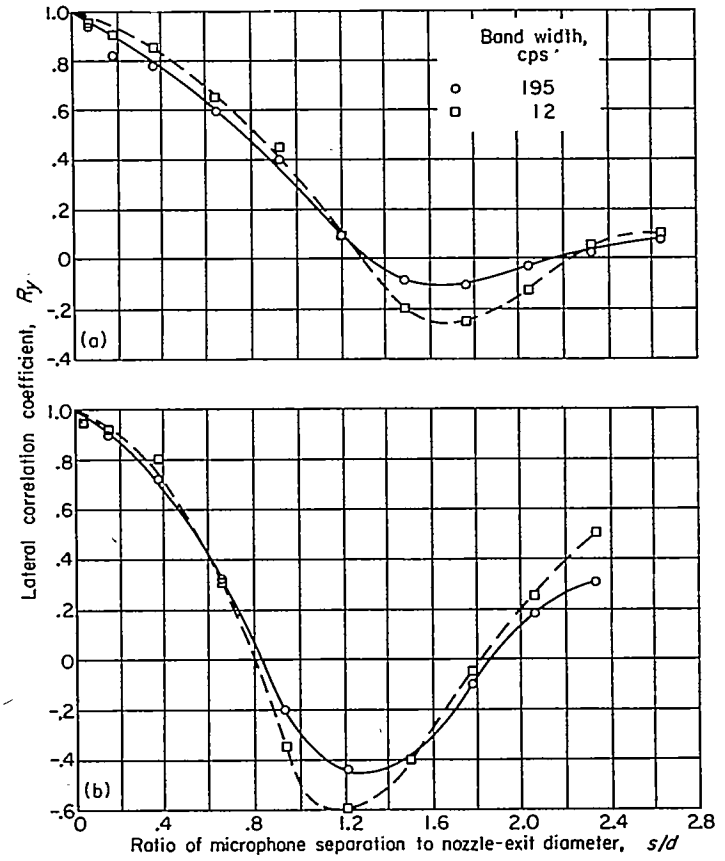

(a) Distance downstream of nozzle exit, x_1, 2.16 nozzle-exit diameters.

(b) Distance downstream of nozzle exit, x_1, 17.3 nozzle-exit diameters.

FIGURE 34.—Lateral correlations of sound pressure at jet boundary for two band widths having midfrequencies of 500 cps.

3. For longitudinal correlations along the jet boundary the first zero-crossing distance was found to increase with distance from the engine up to about 6.5 nozzle-exit diameters. However, at distances of 6.5, 10.8, and 17.3 nozzle-exit diameters downstream from the engine, there was little difference in the first zero-crossing distance.

4. Longitudinal correlations measured 12.1 nozzle-exit diameters from the jet centerline at a distance downstream of 6.5 nozzle-exit diameters from the nozzle exit approached zero asympototically. Farther downstream from the exit (17.3 nozzle-exit diam.), the correlation curves measured 12.1 nozzle-exit diameters from the jet centerline were more nearly like those at the jet boundary.

5. A comparison of the correlation curves obtained at a midfrequency of 500 cps for band widths of 12 and 195 cps showed small effect of band width. The narrow band resulted in increases in the second maximums and minimums, but no significant change occurred in the zero-correlation distance.

6. Correlation curves obtained in free field and on the surface of a plate showed only minor dissimilarity.

7. The distance over which the correlation coefficients were positive was greater for lateral than for longitudinal correlations.

LEWIS FLIGHT PROPULSION LABORATORY
NATIONAL ADVISORY COMMITTEE FOR AERONAUTICS
CLEVELAND, OHIO, *June 6, 1957*

APPENDIX A

SYMBOLS

A	source strength
a	any fluctuating quantity
B	pressure amplitude of sound wave
d	nozzle-exit diameter
E, e	voltages
F	force
f	frequency
K, k	constants
n	a number
P	root-mean-square acoustic pressure
p	instantaneous acoustic pressure
R	correlation coefficient
r	distance from source to receiver
s	microphone separation
T	time period over which signal was integrated
t	time
U	jet velocity
x	axial distance downstream from nozzle exit
x_1	distance along jet boundary from nozzle exit (fig. 20)
y	vertical distance from jet centerline (fig. 20)
z	horizontal distance from jet centerline (fig. 20)
α, β	phase angles
ω	angular frequency
Subscripts:	
o	output
x	longitudinal
x_1	longitudinal along jet boundary
y	lateral

APPENDIX B

CORRELATION COMPUTER

By Channing C. Conger and Donald F. Berg

The correlation computer is a device that is designed to solve by analog methods an equation of the form

$$E_o=\frac{K}{T}\int_0^T e_a(t)e_b(t)\,dt \tag{1}$$

where T is real time, E_o is the output voltage from the computer, and e_a and e_b are the input voltages. The correlation of two voltages may be written as

$$R=\frac{1}{\sqrt{\overline{e_a^2}\,\overline{e_b^2}}}\frac{1}{T}\int_0^T e_a e_b\,dt \tag{2}$$

where the bar indicates the true time average. Therefore, if K is made equal to $1/\sqrt{\overline{e_a^2}\,\overline{e_b^2}}$, then $E_o=R$. If $e_b(t)=e_a(t+\Delta t)$, where Δt is a time delay, then R is termed the autocorrelation coefficient of e_a.

The operation of the computer will be described with reference to figure 35. The two signals whose correlation is to be measured are recorded on a dual-channel tape recorder on ¼-inch magnetic tape. The signals are recorded in periods of from 1 to 30 minutes followed by 10-second intervals during which nothing is recorded on the tape. All tape-recording equipment is commercially available and of instrument quality.

The magnetic tape is played back on a tape handler similar to the one used in recording but with a special playback head arrangement. The playback heads are mounted so that one of the two heads may be translated along the tape with respect to the other. The amount of translation is measured by a micrometer head used to drive the movable playback head. The maximum head motion is ¾ inch, and this motion may be measured to an accuracy of 1×10^{-4} inch by means of a vernier on the micrometer head. The tape speed used on playback is 15 inches per second. Therefore, the adjustment allows an adjustable delay of from 0 to 50 milliseconds to be introduced between the signals from the two playback heads. This adjustable delay is used in the determination of autocorrelation functions as described previously. For cross correlations (as from two microphones), the delay is adjusted to zero.

The compensation amplifiers receive the two signals from the playback heads. The gain characteristics of these amplifiers have been adjusted by means of passive filters to compensate for the frequency characteristics of the recording system. They also serve to correct for the frequency response of the playback heads and to amplify the signals to a level suitable for use by the remainder of the circuitry. From the compensating amplifiers, the signals go to the variable-gain amplifiers, as shown in the block diagram. The adjustable-gain feature of these amplifiers is used to set the scaling coefficient K of equation (1).

The switching circuit (indicated in fig. 35) allows switching the inputs to the electronic multiplier in order to obtain the products listed in table I.

From the switching circuit, the two signals are applied to the electronic multiplier. The multiplier produces an output voltage proportional to the instantaneous product

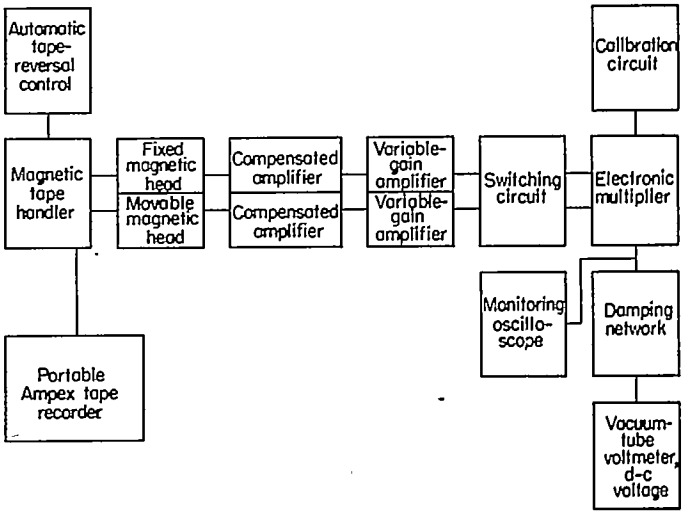

FIGURE 35.—Block diagram of correlation computer.

of the input voltages. The product voltage is applied to resistance-capacitance averaging circuit of conventional design. The average amplitude of the product voltage is then read from the vacuum-tube voltmeter.

When used for autocorrelation measurements, the computer is usually adjusted so that the correlation may be read directly from the voltmeter. The adjustment consists of the following: The heads are adjusted until zero time lag is produced; therefore, the correlation is unity. Then, the gain of the variable-gain amplifiers is adjusted until the output of the multiplier indicates 1 volt full scale on the voltmeter. With this initial setting, the autocorrelation coefficient may be read directly from the voltmeter dial as a function of the time delay obtained by adjusting the movable head.

Two blocks of figure 35 remain to be described, the calibration circuit and the tape-reversal control. The calibration circuit provides appropriate alternating-current and direct-current voltages that may be switched into the electronic multiplier. These voltages are used for calibration and adjustment of the multiplier prior to use.

The tape-reversal control is used to operate automatically the tape handler. The control uses the 10-second blank intervals at the end and beginning of a section of recorded data on the tape to stop automatically, rewind, and restart the tape handler. Use of the controller, therefore, allows a section of the tape to be played back repeatedly without attention from the operator and produces the effect of a loop of tape without the necessity of cutting and splicing the tape.

Complete circuits of the correlation computer showing the construction of electronic portions of the equipment (and the amplifier response curves) are presented in figures 36 to 43.

REFERENCES

1. Bolt, Richard H.: Aircraft Noise and Its Relation to Man. Paper presented at Inst. Aero. Sci. meeting, Cleveland (Ohio), Mar. 12, 1954.
2. Bolt, Richard H.: Aircraft Noise Problem. Jour. Acoustical Soc. Am., vol. 25, no. 3, May 1953, pp. 363–366.
3. Stevens, K. N.: A Survey of Background and Aircraft Noise in Communities Near Airports. NACA TN 3379, 1954.
4. Hubbard, Harvey H.: A Survey of the Aircraft Noise Problem with Special Reference to Its Physical Aspects. NACA TN 2701, 1952.
5. Miles, John W.: On Structural Fatigue Under Random Loading. Jour. Aero. Sci., vol. 21, no. 11, Nov. 1954, pp. 753–762.
6. Powell, Alan: The Problem of Structural Failure Due to Jet Noise. Oscillation Sub-Committee, Rep. No. 17514, British ARC, Mar. 29, 1955.
7. Westley, R., and Lilley, G. M.: An Investigation of the Noise Field from a Small Jet and Methods for Its Reduction. Rep. No. 53, The College of Aero. (Cranfield), Jan. 1952.
8. Lassiter, Leslie W., and Hubbard, Harvey H.: The Near Noise Field of Static Jets and Some Model Studies of Devices for Noise Reduction. NACA Rep. 1261, 1956. (Supersedes NACA TN 3187.)
9. Greatrex, F. B.: Engine Noise. Joint Symposium on Aero. Acoustics (London), May 21, 1953.
10. Greatrex, F. B.: Jet Noise. Preprint No. 559, Inst. Aero. Sci., June 1955.
11. Lighthill, M. J.: On Sound Generated Aerodynamically. I. General Theory. Proc. Roy. Soc. (London), ser. A, vol. 211, no. 1107, Mar. 20, 1952, pp. 564–587.
12. Lighthill, M. J.: On Sound Generated Aerodynamically. II. Turbulence as a Source of Sound. Proc. Roy. Soc. (London), ser. A, vol. 222, no. 1148, Feb. 23, 1954, pp. 1–32.
13. Callaghan, Edmund E., and Coles, Willard D.: Far Noise Field of Air Jets and Jet Engines. NACA Rep. 1329, 1957.
14. Lassiter, Leslie W., and Hubbard, Harvey H.: Experimental Studies of Noise from Subsonic Jets in Still Air. NACA TN 2757, 1952.
15. Laurence, James C.: Intensity, Scale, and Spectra of Turbulence in Mixing Region of Free Subsonic Jet. NACA Rep. 1292, 1957. (Supersedes NACA TN's 3561 and 3576.)
16. Mawardi, Osman K.: On the Spectrum of Noise from Turbulence. Jour. Acoustic Soc. Am., vol. 27, no. 3, May 1955, pp. 442–445.
17. Corrsin, Stanley, and Uberoi, Mahinder S.: Further Experiments on the Flow and Heat Transfer in a Heated Turbulent Air Jet. NACA Rep. 998, 1950. (Supersedes NACA TN 1865.)
18. Gooderum, Paul B., Wood, George P., and Brevoort, Maurice J.: Investigation with an Interferometer of the Turbulent Mixing of a Free Supersonic Jet. NACA Rep. 963, 1950. (Supersedes NACA TN 1857.)
19. Hubbard, H. H., and Lassiter, L. W.: Experimental Studies of Jet Noise. Jour. Acoustic Soc. Am., vol. 25, no. 3, May 1953, pp. 381–384.
20. Laurence, James C., and Landes, L. Gene: Auxiliary Equipment and Techniques for Adapting the Constant-Temperature Hot-Wire Anemometer to Specific Problems in Air-Flow Measurements. NACA TN 2843, 1952.

TABLE I.—SWITCH POSITION FOR SWITCHING CIRCUIT

Switch position	Meter signal proportional to (a)
1	XYZ
2	YZ^2
3	XZ^2
4	XY^2
5	ZY^2
6	ZX^2
7	YX^2
8	YZ
9	XY
10	XZ
11	Z^2
12	Y^2
13	X^2

[a]Fluctuating quantities.

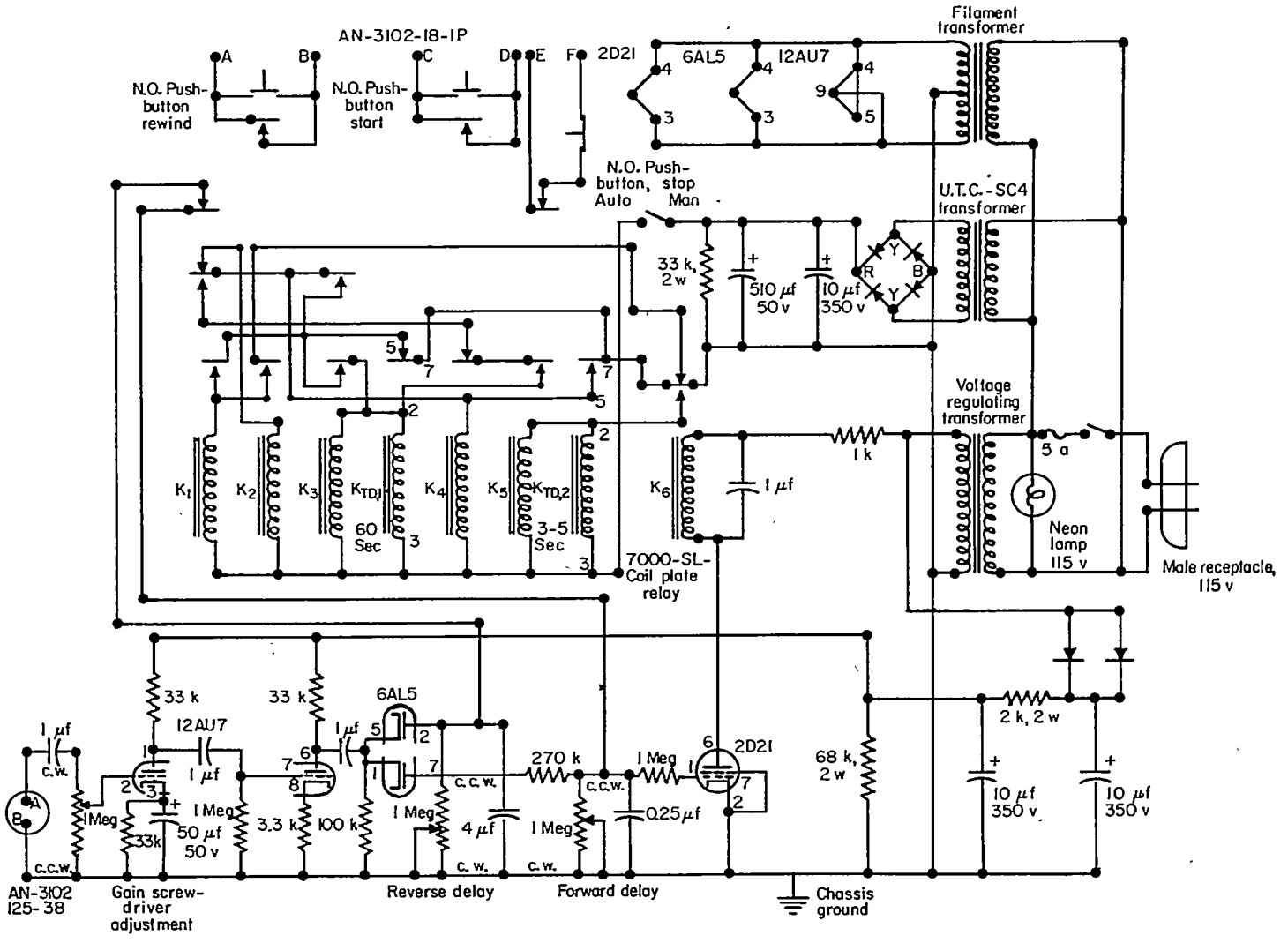

FIGURE 36.—Automatic tape-reversal mechanism.

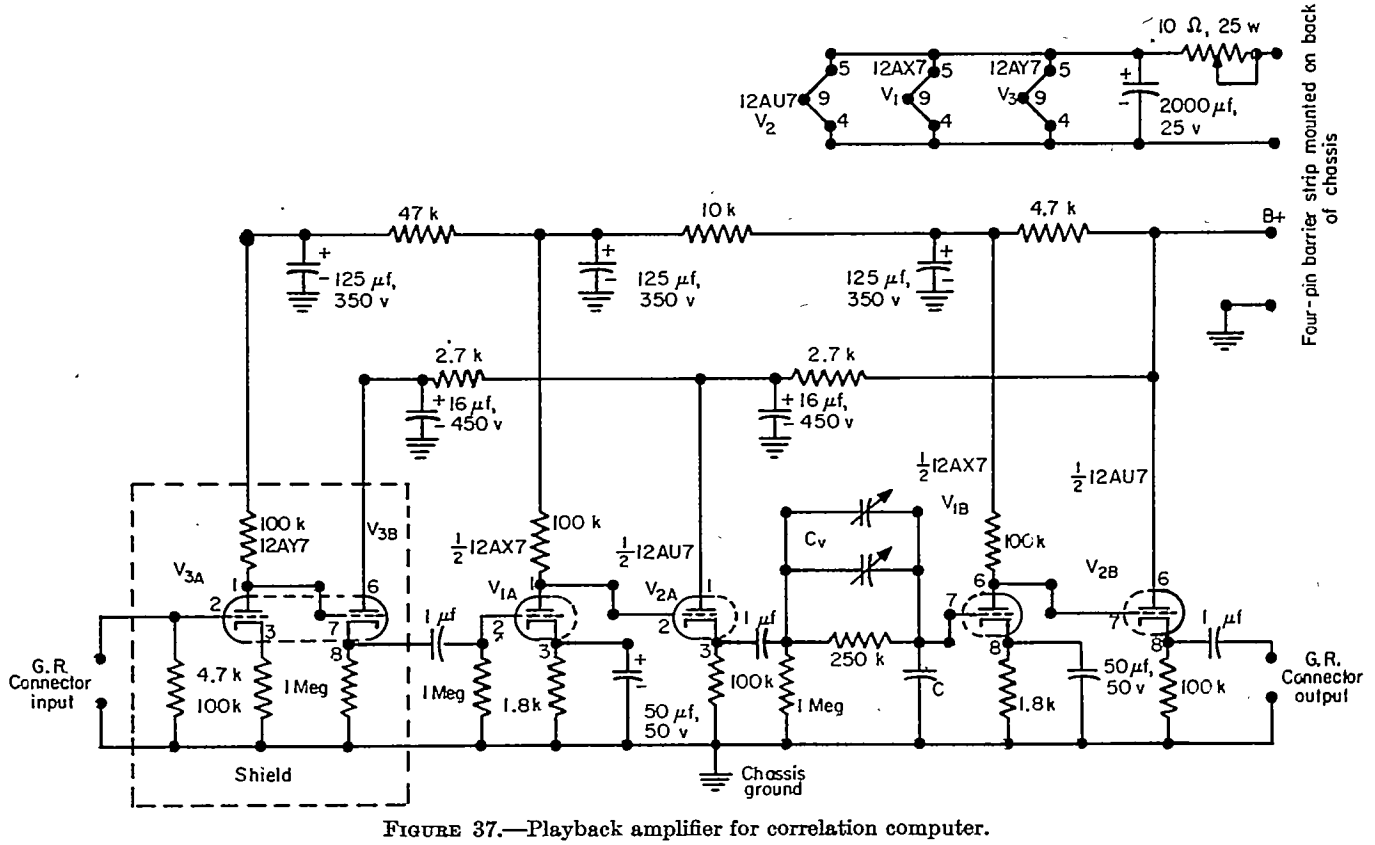

FIGURE 37.—Playback amplifier for correlation computer.

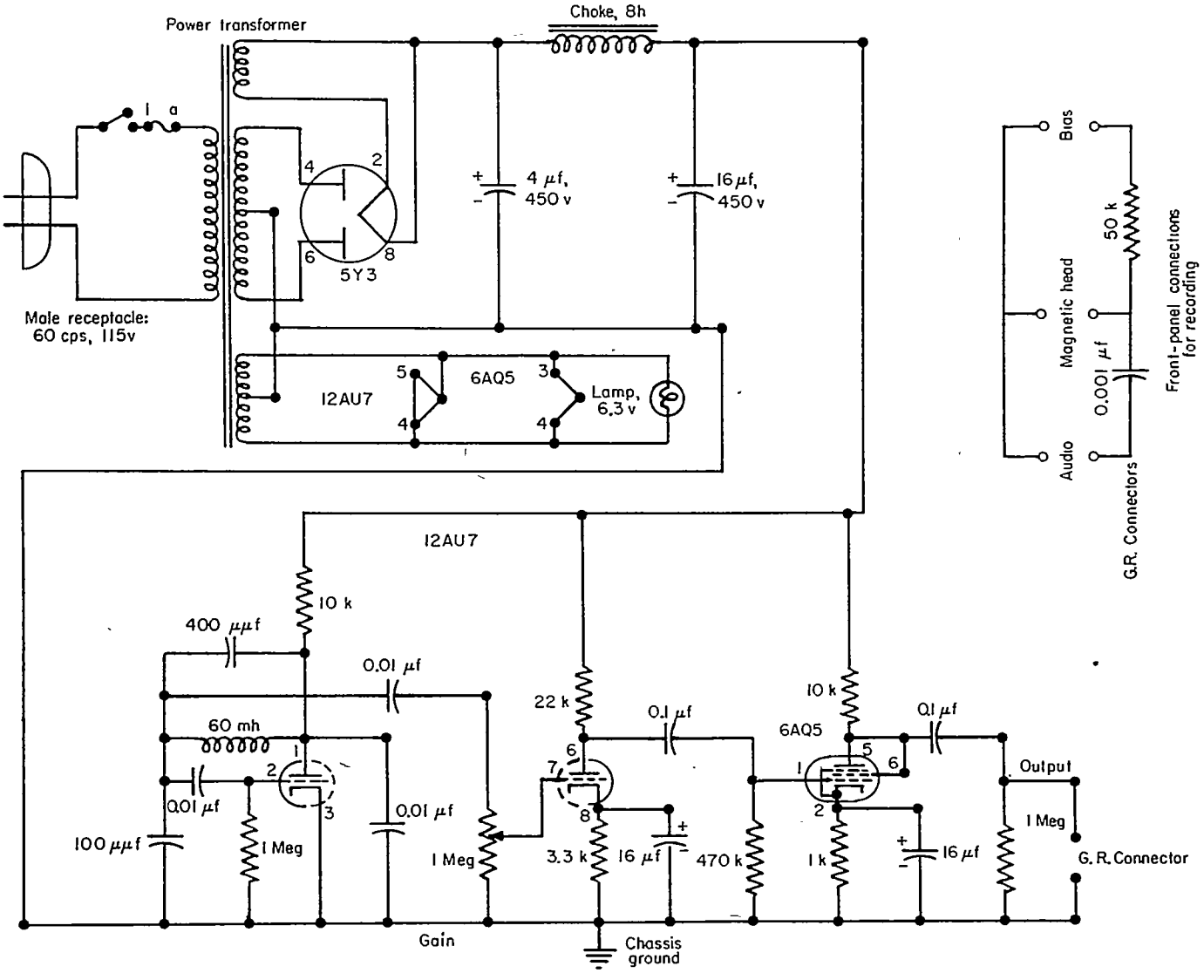

FIGURE 38.—Bias oscillator for recording.

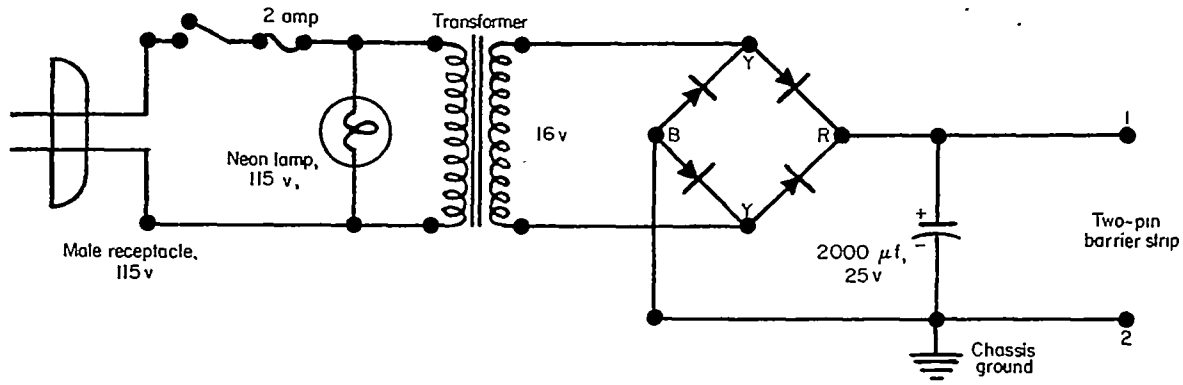

(a)

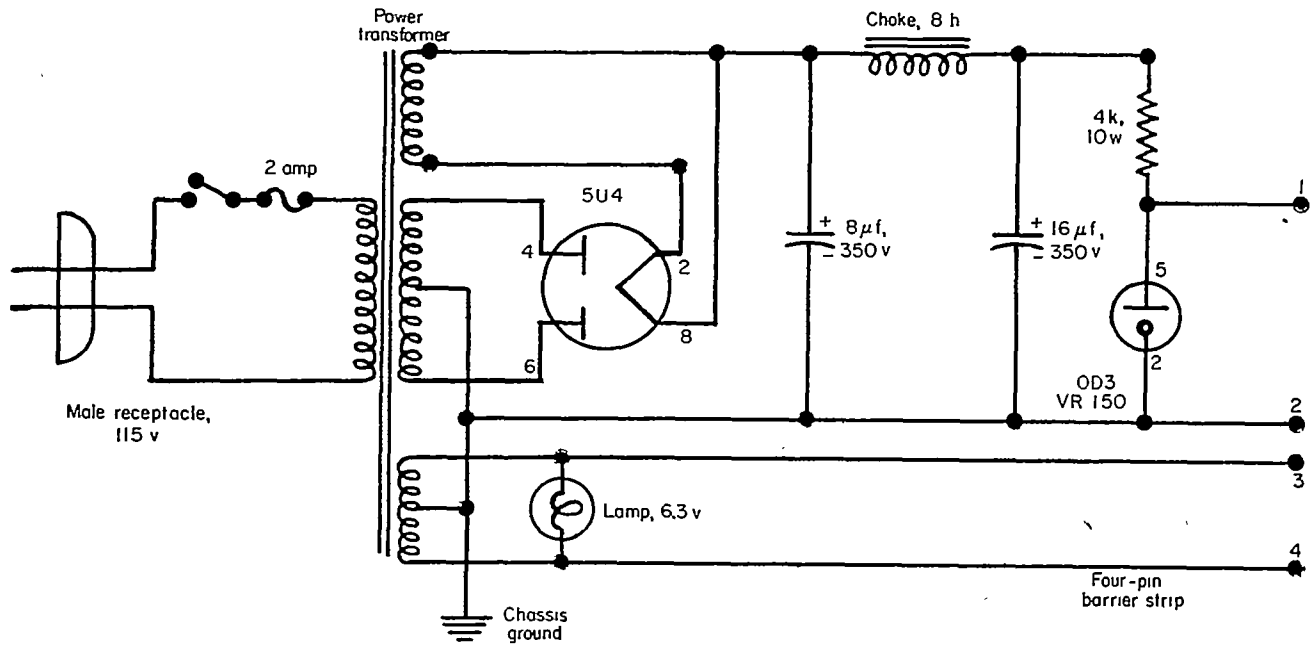

(b)

(a) Filament.
(b) Plate power.

FIGURE 39.—Voltage supply for playback amplifiers.

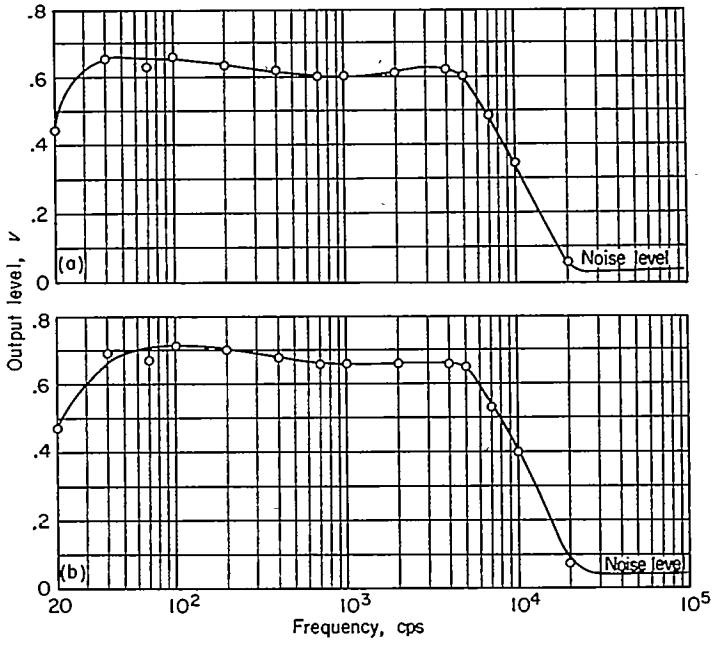

(a) Top amplifier.
(b) Lower amplifier.

FIGURE 40.—Over-all response of playback system (amplifiers and head) to a flat signal recorded on Ampex equipment.

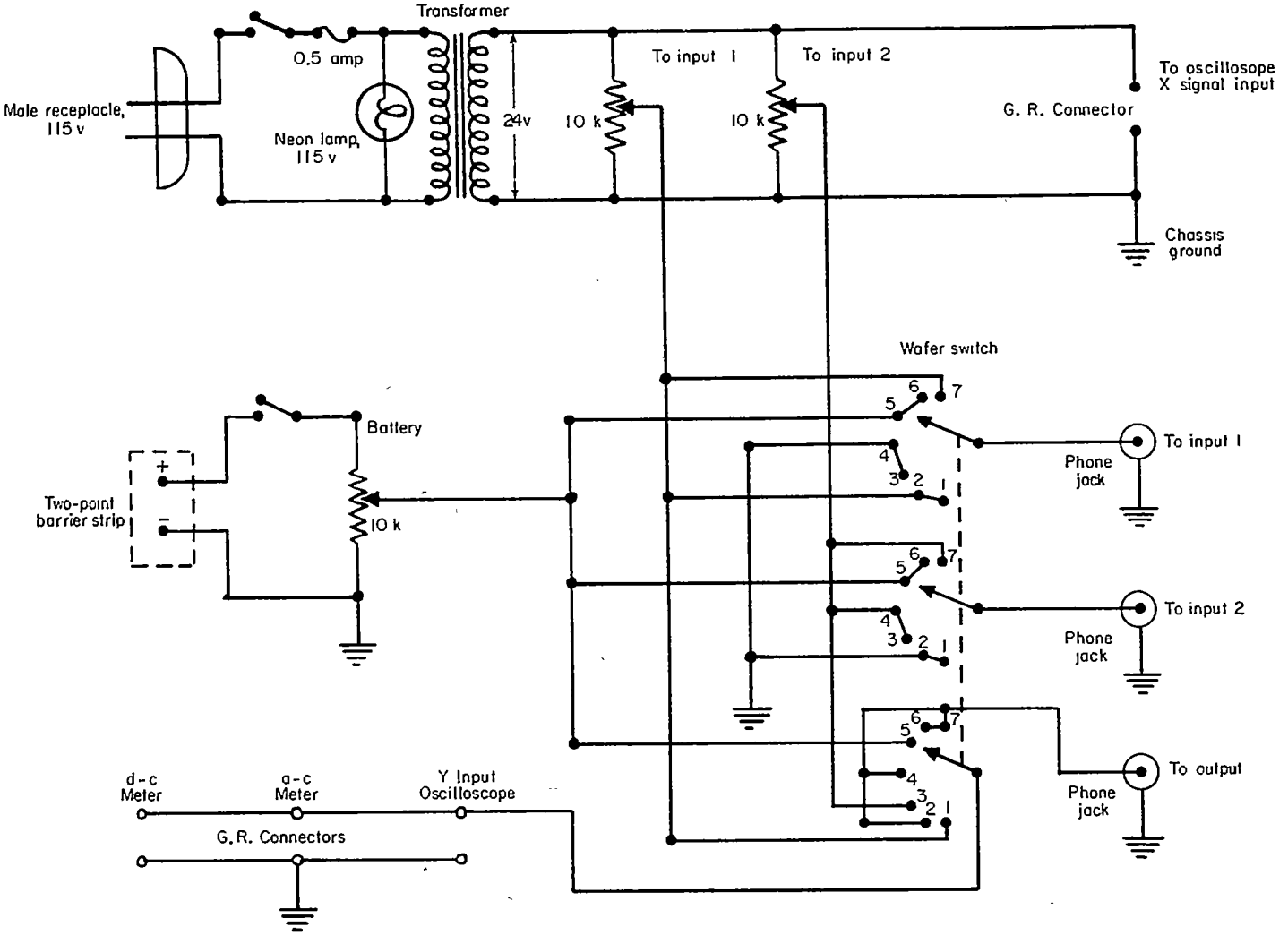

FIGURE 41.—Calibration circuit for Philbrick multiplier

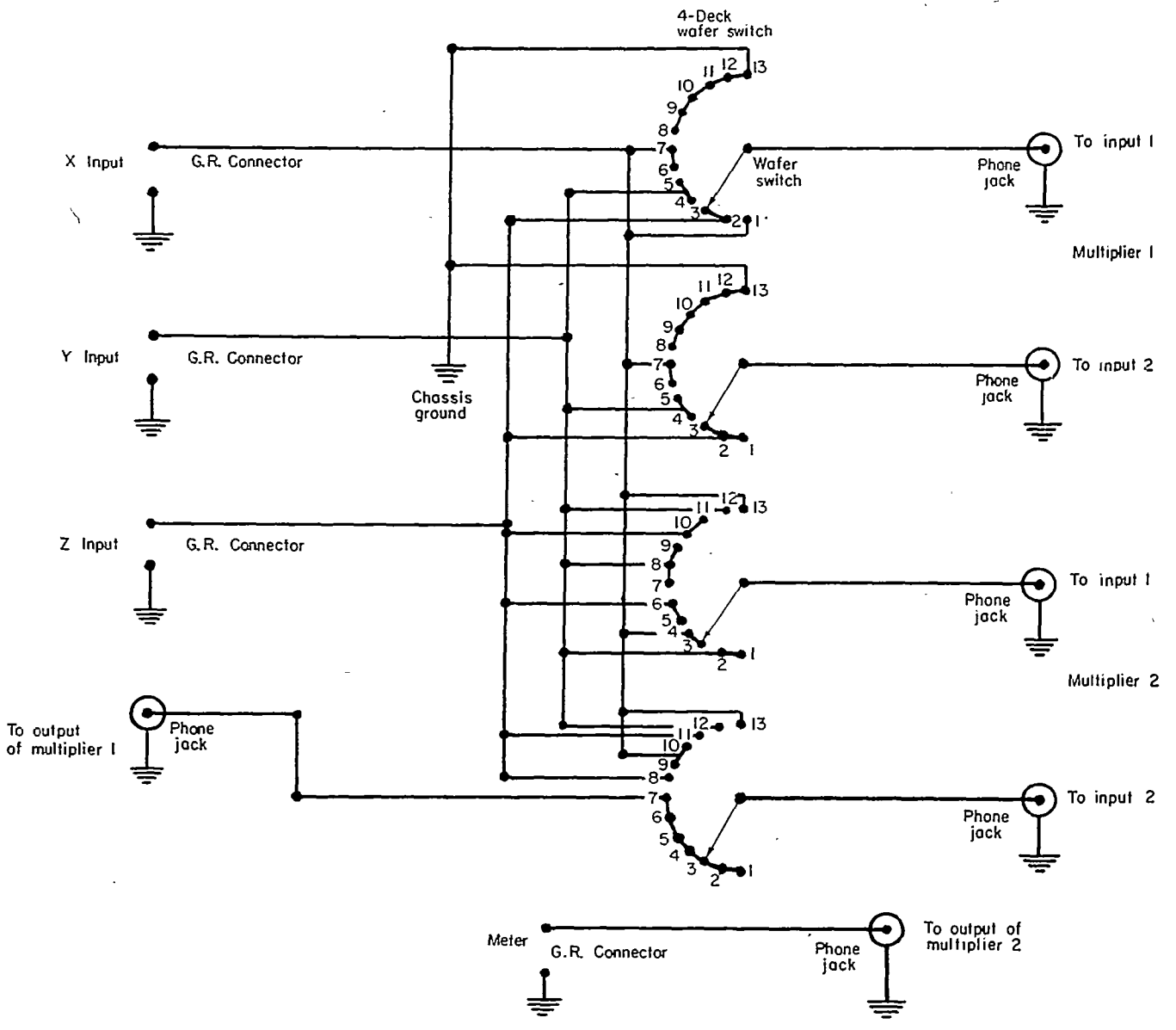

FIGURE 42.—Switching circuit for Philbrick multiplier for triple correlation.

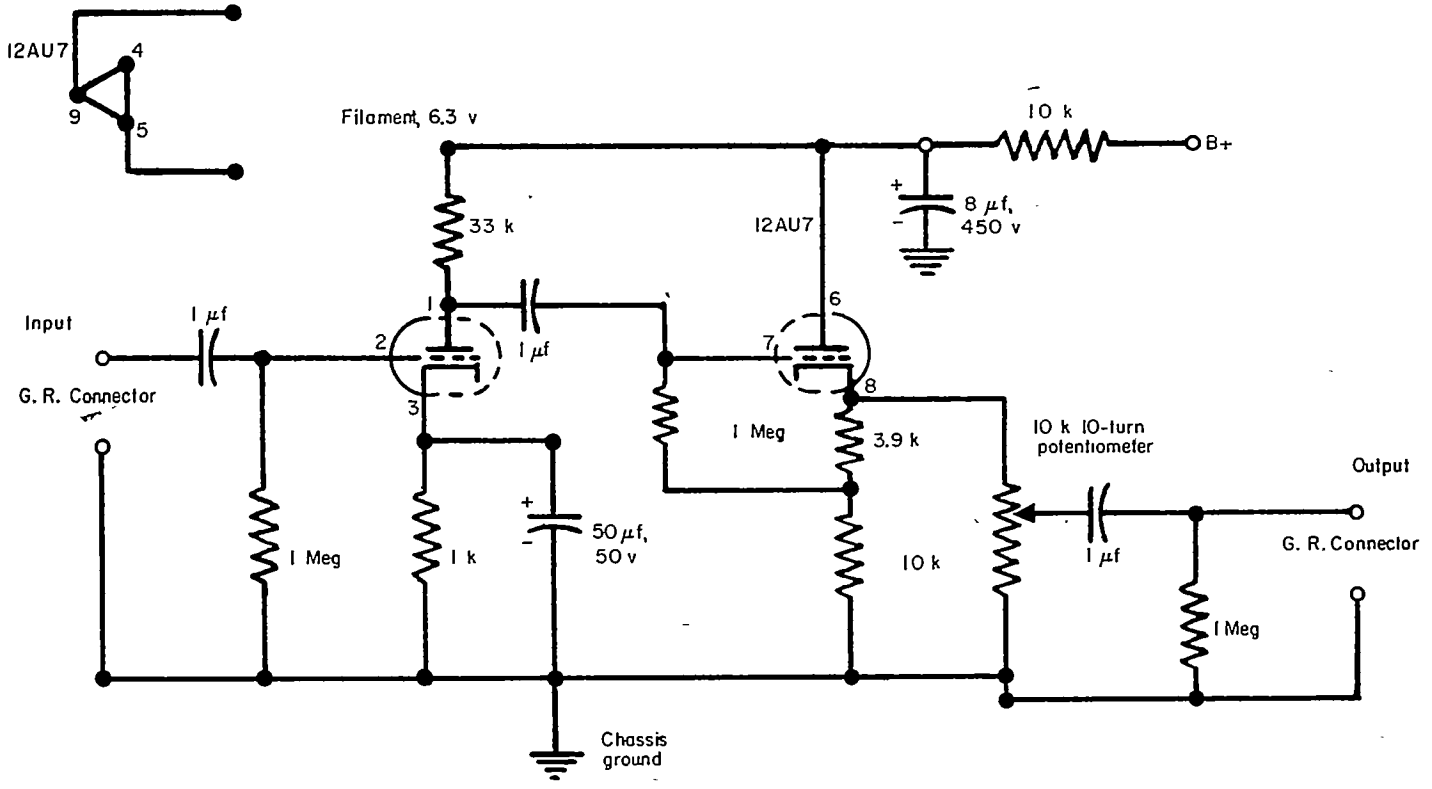

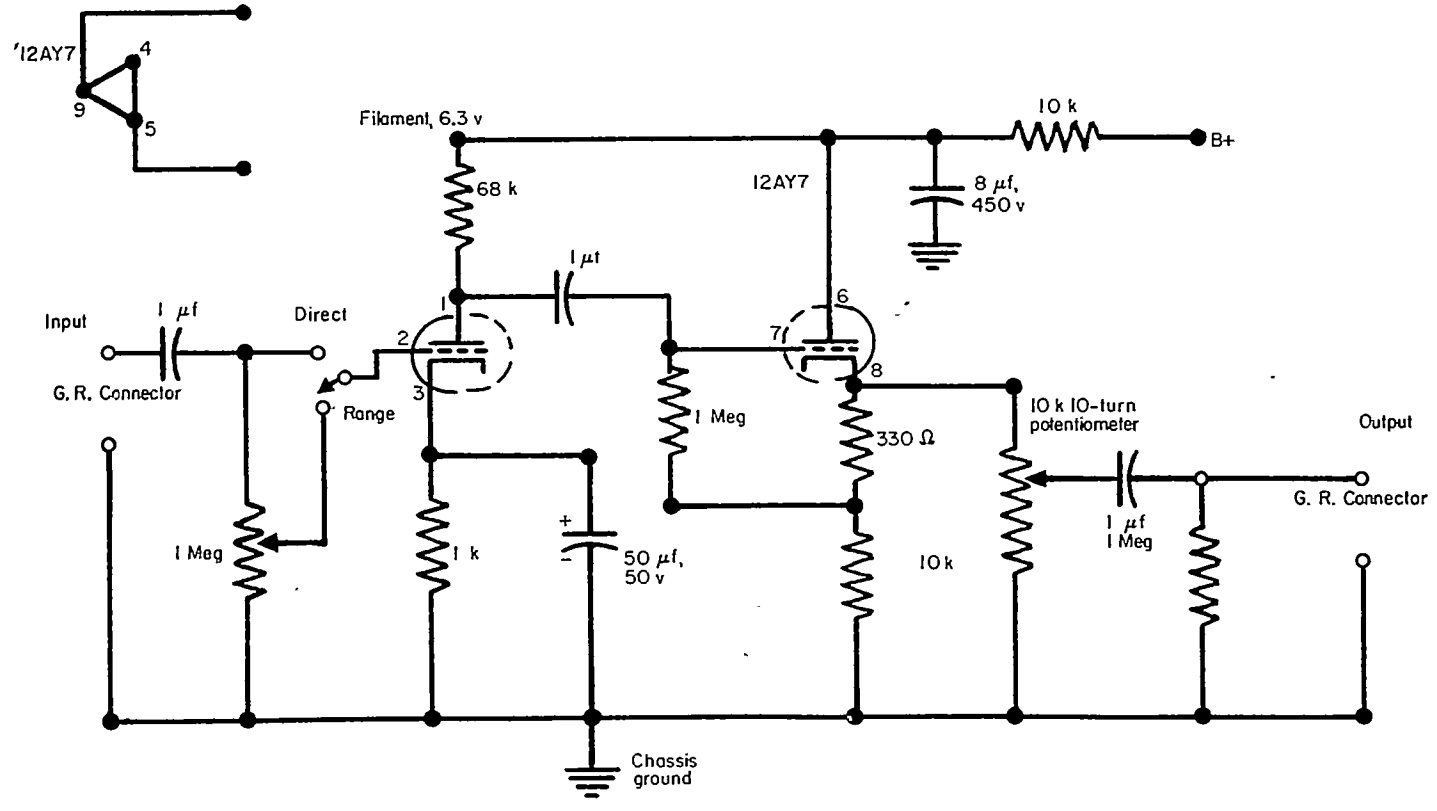

FIGURE 43.—Preamplifier circuits.